Article

Gasdermin E suppresses tumour growth by activating anti-tumour immunity

https://doi.org/10.1038/s41586-020-2071-9

Received: 18 July 2019

Accepted: 10 January 2020

Published online: 11 March 2020

Check for updates

Zhibin Zhang[1,2,12]✉, Ying Zhang[1,2,12], Shiyu Xia[1,3], Qing Kong[4,5], Shunying Li[6], Xing Liu[1,2,7], Caroline Junqueira[1,2,8], Karla F. Meza-Sosa[1,2,9], Temy Mo Yin Mok[1,2,10], James Ansara[1,2], Satyaki Sengupta[2,11], Yandan Yao[6], Hao Wu[1,3] & Judy Lieberman[1,2]✉

Cleavage of the gasdermin proteins to produce pore-forming amino-terminal fragments causes inflammatory cell death (pyroptosis)[1]. Gasdermin E (GSDME, also known as DFNA5)—mutated in familial ageing-related hearing loss[2]—can be cleaved by caspase 3, thereby converting noninflammatory apoptosis to pyroptosis in GSDME-expressing cells[3–5]. *GSDME* expression is suppressed in many cancers, and reduced GSDME levels are associated with decreased survival as a result of breast cancer[2,6], suggesting that GSDME might be a tumour suppressor. Here we show that 20 of 22 tested cancer-associated GSDME mutations reduce GSDME function. In mice, knocking out *Gsdme* in GSDME-expressing tumours enhances, whereas ectopic expression in *Gsdme*-repressed tumours inhibits, tumour growth. This tumour suppression is mediated by killer cytotoxic lymphocytes: it is abrogated in perforin-deficient mice or mice depleted of killer lymphocytes. GSDME expression enhances the phagocytosis of tumour cells by tumour-associated macrophages, as well as the number and functions of tumour-infiltrating natural-killer and $CD8^+$ T lymphocytes. Killer-cell granzyme B also activates caspase-independent pyroptosis in target cells by directly cleaving GSDME at the same site as caspase 3. Uncleavable or pore-defective GSDME proteins are not tumour suppressive. Thus, tumour GSDME acts as a tumour suppressor by activating pyroptosis, enhancing anti-tumour immunity.

Evidence that GSDME might act as a tumour suppressor (including epigenetic *GSDME* inactivation by promoter DNA methylation in many cancer lines and primary cancers[2,6]; suppression by GSDME of colony formation and cell proliferation in gastric cancer, melanoma and colorectal cancer and of breast-cancer invasiveness; and worse five-year survival and increased metastases from breast cancers that poorly express *GSDME*[2,6]) prompted us to probe whether and how GSDME might function as a tumour suppressor. Induction of inflammatory cell death in GSDME-expressing cancers subjected to intrinsic stresses (hypoxia or endoplasmic-reticulum stress) or extrinsic challenges (chemotherapy, radiation or attack by cytotoxic lymphocytes) that activate caspase 3 could have a marked effect on the tumour microenvironment, immune-cell recruitment and function, and tumour growth. Here we show that GSDME in tumours suppresses tumour growth by increasing the anti-tumour functions of tumour-infiltrating natural-killer (NK) and $CD8^+$ T killer lymphocytes.

GSDME converts apoptosis to pyroptosis

We first found that *Gsdme* messenger RNA and/or protein in seven mouse tumour cell lines was within the range seen in primary breast cancers and colorectal cancer in The Cancer Genome Atlas (TCGA) database (https://www.cancer.gov/tcga) (Extended Data Fig. 1a–c). *Gsdme* was knocked out in two highly expressing mouse lines, namely EMT6 triple negative breast cancer and CT26 colorectal cancer (Extended Data Fig. 1d–g), and one human neuroblastoma line, namely SH-SY5Y (Extended Data Fig. 1h). Moreover, *Gsdme* or *GSDME* was stably expressed in two poorly expressing mouse cancer cell lines—B16-F10 melanoma (hereafter referred to as B16) and 4T1E triple negative breast cancer (Extended Data Fig. 1i, j)—and in a human cervical carcinoma cell line (HeLa) (Extended Data Fig. 1k).

To examine the effect of GSDME on cell death, we treated B16 cells that were expressing empty vector or overexpressing mouse GSDME (mGSDME) with raptinal, a rapid caspase 3 activator[7]. We found that

[1]Program in Cellular and Molecular Medicine, Boston Children's Hospital, Boston, MA, USA. [2]Department of Pediatrics, Harvard Medical School, Boston, MA, USA. [3]Department of Biological Chemistry and Molecular Pharmacology, Harvard Medical School, Boston, MA, USA. [4]Department of Cancer Biology, Dana-Farber Cancer Institute, Boston, MA, USA. [5]Department of Genetics, Harvard Medical School, Boston, MA, USA. [6]Breast Tumor Center, Sun Yat-Sen Memorial Hospital, Sun Yat-Sen University, Guangzhou, China. [7]The Center for Microbes, Development and Health, Key Laboratory of Molecular Virology and Immunology, Institut Pasteur of Shanghai, Chinese Academy of Sciences, Shanghai, China. [8]René Rachou Institute, Oswaldo Cruz Foundation, Belo Horizonte, Brazil. [9]Laboratorio de Neuroimmunobiología, Departamento de Medicina Molecular y Bioprocesos, Instituto de Biotecnología, Universidad Nacional Autónoma de México, Cuernavaca, Mexico. [10]Department of Biomedical Sciences, City University of Hong Kong, Hong Kong, Hong Kong. [11]Department of Pediatric Oncology, Dana-Farber Cancer Institute, Boston, MA, USA. [12]These authors contributed equally: Zhibin Zhang, Ying Zhang. ✉e-mail: zhibin.zhang@childrens.harvard.edu; judy.lieberman@childrens.harvard.edu

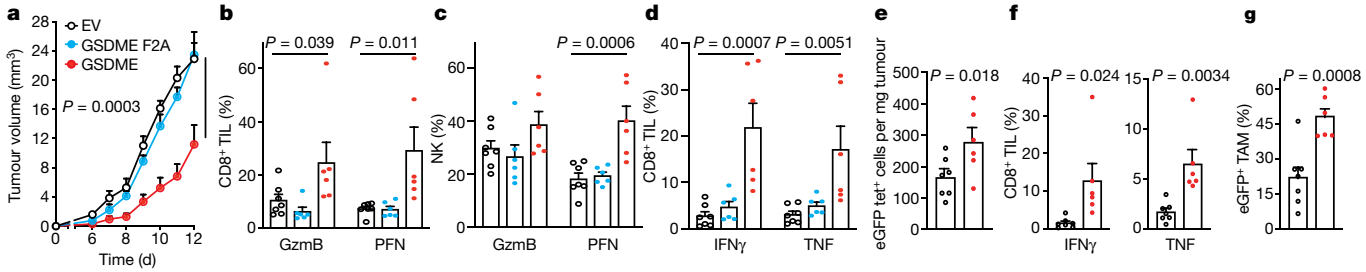

Fig. 1 | Ectopic expression of pore-forming, but not inactive, GSDME reduces tumour growth and enhances tumour immune responses. **a**–**d**, Orthotopically implanted 4T1E cells stably expressing wild-type mGSDME ($n = 6$ mice per group), inactive F2A mGSDME ($n = 6$ mice per group) or empty vector (EV; $n = 7$ mice per group) were analysed for tumour growth (**a**) and TIL function (**b**–**d**). **b**–**d**, Percentages of CD8⁺ (**b**) and NK (**c**) TILs expressing GzmB or PFN, and of CD8⁺ TILs producing IFNγ or TNF induced by PMA and ionomycin (**d**). **e**–**g**, Anti-tumour immunity after orthotopic implantation of 4T1E cells stably expressing eGFP and then stably transduced to express mGSDME or empty vector ($n = 7$ mice per group). **e**, Mean numbers of tumour-specific GFP-tetramer-positive (tet⁺) CD8⁺ TILs per milligram of tumour. **f**, Percentage of CD8⁺ TILs activated by eGFP peptide to produce IFNγ or TNF. **g**, Percentage of GFP⁺ tumour-associated macrophages (TAMs) that phagocytosed tumour cells. **a**, The area under the curve of tumour growth curves was compared by one-way analysis of variance (ANOVA) with Holm–Sidak correction for type I error. **b**–**d**, Comparisons were calculated by one-way ANOVA using the Holm–Sidak method for multiple comparisons. **e**–**g**, Comparisons were calculated by two-tailed Student's *t*-test. Data shown are mean + s.e.m. and are representative of two independent experiments. Each dot represents data from an individual mouse.

mGSDME did not alter cell-death kinetics and extent, as measured by annexin V/propidium iodide staining (Extended Data Fig. 2a). Raptinal did not trigger pyroptosis in B16 cells expressing empty vector (with pyroptosis being assessed by uptake of SYTOX green and release of lactate dehydrogenase (LDH)), but did so in mGSDME-overexpressing cells after roughly 40 min (Extended Data Fig. 2b, c). Pyroptotic ballooning cell membranes and SYTOX green uptake were detected by time-lapse fluorescence microscopy in mGSDME-overexpressing cells only (Extended Data Fig. 2d and Supplementary Videos 1, 2). Empty-vector cells instead became apoptotic (detached and shrunken, with membrane blebbing). After adding raptinal, caspase-3-mediated cleavage was detected independently of mGSDME overexpression, beginning within 20 min, and mGSDME cleavage was detected coincidently if mGSDME was expressed (Extended Data Fig. 2e). Although raptinal did not appreciably change cellular levels of the nuclear protein HMGB1, only mGSDME-overexpressing B16 cells released HMGB1. Similarly, raptinal or tumour-necrosis-factor (TNF)-related apoptosis-inducing ligand (TRAIL) converted apoptosis to pyroptosis only in HeLa cells that overexpressed human GSDME (hGSDME) (Extended Data Fig. 2f–i and Supplementary Videos 3, 4). Thus, GSDME is cleaved rapidly after caspase 3 activation and then permeabilizes the cell membrane, converting apoptosis to pyroptosis, as previously reported[3,4].

Loss-of-function *GSDME* mutations in cancer

If GSDME is a tumour suppressor, then some GSDME-expressing cancers might have loss-of-function (LOF) mutations. We examined the TCGA database of single-nucleotide polymorphisms in primary cancers for GSDM mutations (Extended Data Fig. 3a). *GSDME* and *GSDMC* had the most mutations, and there were more *GSDME* mutations around the caspase 3 cleavage site. *GSDME* single-nucleotide polymorphisms in the N terminus were mapped onto the GSDME N-terminal pore, modelled on the basis of the mouse GSDMA3 N terminus[8] (Extended Data Fig. 3b, e). We expressed 18 GSDME N-terminal conserved-site mutants in HEK293T cells and tested the cells for pyroptosis. All of the mutant proteins were well-expressed (Extended Data Fig. 4c, f), and 16 of 18 cancer-associated single-nucleotide polymorphisms substantially reduced LDH release compared with the wild-type GSDME N terminus (Extended Data Fig. 3d, g), suggesting that some cancer-associated GSDME N-terminal mutations cause LOF. Mutations in the globular domain close to the oligomerization and cell-membrane-binding sites had the largest effect. Four premature stop mutants (GSDME 1–46, 1–210, 1–451 or 1–491) also did not cause pyroptosis in HEK293T cells, although some of the mutated proteins (1–451 and 1–491) may have been unstable (Extended Data Fig. 3h–l). We verified a previously described[3] LOF F2A mutation (single-letter amino-acid code) (Extended Data Fig. 3m, n). F2, D18 and P212 are conserved between human and mouse GSDME. Expression of mGSDME N termini with an F2A, D18V or P212L mutation in HEK293T cells, or of F2A or P212L full-length mGSDME mutants in 4T1E cells, markedly reduced spontaneous or raptinal-induced pyroptosis, respectively, compared with unmutated mGSDME (Extended Data Fig. 3o, r). Thus, 20 of 22 (91%) studied cancer-related *GSDME* mutations cause LOF.

GSDME affects tumour growth and immunity

EMT6 (Extended Data Fig. 4a–e) and CT26 (Extended Data Fig. 4f–j) tumours knocked out for *Gsdme* grew much faster in immunocompetent mice than did tumours expressing endogenous *Gsdme* (Extended Data Fig. 4a, f). The tumour microenvironment of *Gsdme*$^{-/-}$ EMT6 tumours had fewer CD8⁺ T and NK cells and a trend towards fewer tumour-associated macrophages (Extended Data Fig. 4b). Tumour-infiltrating lymphocytes (TILs: CD8⁺ T and NK cells) from *Gsdme*$^{-/-}$ EMT6 and CT26 tumours also expressed less granzyme B (GzmB) and/or perforin (PFN) (Extended Data Fig. 4c, d, g, h), and produced less interferon-γ (IFNγ) and TNF after stimulation with phorbol 12-myristate 13-acetate (PMA) and ionomycin (Extended Data Fig. 4e, i, j). Thus, endogenous GSDME suppresses tumour growth and promotes TIL function.

Conversely, ectopic mGSDME expression in 4T1E (Fig. 1 and Extended Data Fig. 5) and B16 (Extended Data Fig. 6) cells markedly inhibited tumour growth (Fig. 1a and Extended Data Fig. 6a). GSDME-expressing 4T1E tumours had substantially more tumour-infiltrating NK cells and tumour-associated macrophages, but not CD8⁺ TILs (Extended Data Fig. 5a). More NK and CD8⁺ TILs expressed GzmB and PFN (Fig. 1b, c) and more CD8⁺ TILs produced IFNγ and TNF (Fig. 1d). 4T1E tumours overexpressing F2A or P212L LOF mutants of GSDME did not have more functional TILs (Fig. 1a–d, Extended Data Fig. 5a and data not shown). Similarly, increased TIL numbers and function were observed in B16 tumours overexpressing wild-type but not F2A GSDME (Extended Data Fig. 6b–d). Thus, GSDME pores were required for tumour-suppressive immune enhancement.

Ectopic mGSDME expression in 4T1E tumours producing enhanced green fluorescent protein (eGFP) (Fig. 1e–g and Extended Data Fig. 5b–e)

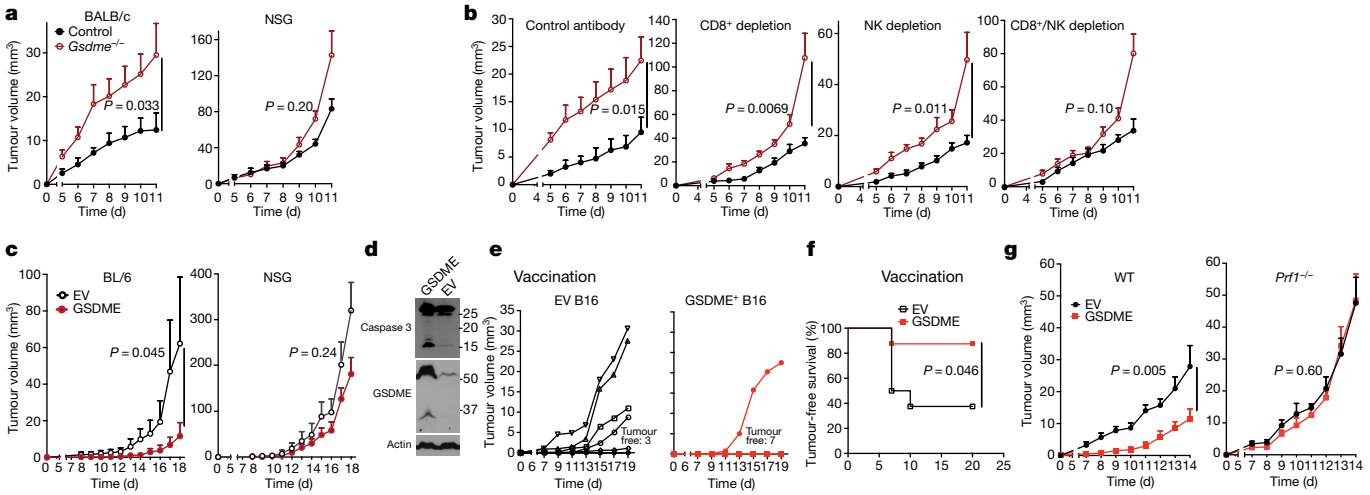

Fig. 2 | GSDME-mediated tumour inhibition depends on cytotoxic lymphocytes. a, **b**, Growth of control or *Gsdme*$^{-/-}$ EMT6 cells in BALB/c mice (left, $n = 8$ mice per group) and NSG mice (right, control $n = 7$ mice per group; *Gsdme*$^{-/-}$ $n = 8$ mice per group) (**a**); or in BALB/c mice treated with an isotype control antibody ($n = 6$ mice per group) or depleted of CD8$^+$ T cells ($n = 8$ mice per group), NK cells ($n = 7$ mice per group) or both ($n = 8$ mice per group) (**b**). Antibody depletion (Extended Data Fig. 7a) was verified on day 3 after tumour challenge and on day 11 at necropsy (Extended Data Fig. 7b, c). **c**, Growth of empty vector or mGSDME-overexpressing B16 cells in C57BL/6 mice (left, empty vector $n = 5$ mice per group, mGSDME $n = 8$ mice per group) and NSG mice (right, $n = 6$ mice per group). **d**–**f**, B16 vaccination model. C57BL/6 mice were vaccinated in the left flank with empty vector or GSDME-positive B16 cells and challenged 10 days later with empty vector B16 cells in the right flank ($n = 8$ mice per group). Shown are immunoblots of lysates of representative left-flank tumours at necropsy probed for caspase 3, GSDME and actin loading control (**d**), right-flank tumour growth (**e**) and tumour-free survival (**f**). **g**, Comparison of growth of orthotopic empty vector and mGSDME-positive 4T1E tumours in wild-type (WT) ($n = 7$ mice per group) and *Prf1*$^{-/-}$ (empty vector $n = 6$ mice per group, mGSDME $n = 7$ mice per group) BALB/c mice. The area under the growth curves was compared by two-tailed Student's *t*-test. A log-rank test was used for survival analysis. Data are mean + s.e.m. and are representative of two independent experiments.

also reduced tumour growth (Extended Data Fig. 5d). In this model, tumour-specific CD8$^+$ TILs could be examined using GFP tetramers. GSDME markedly increased the number of CD8$^+$ TILs that stained with GFP tetramers (Fig. 1e). Tetramer-positive TILs in GSDME-overexpressing tumours expressed substantially more PFN (Extended Data Fig. 5e), and also produced more cytokines after stimulation with GFP peptide (Fig. 1f). Tumour-associated macrophages in mGSDME-expressing tumours were twice as likely to be GFP-positive, indicating increased in vivo phagocytosis of tumour cells (Fig. 1g).

Killer lymphocytes mediate tumour suppression

Enhanced immune function in mGSDME-expressing tumours suggests that tumour inhibition might be immune-mediated. To investigate this hypothesis, we compared GSDME-expressing and *Gsdme*$^{-/-}$ EMT6 tumours in wild-type BALB/c mice and in NSG mice (for 'non-obese diabetic (NOD), severe combined immunodeficient (SCID), interleukin-2-receptor-γ null'), the latter of which lack mature lymphocytes (Fig. 2a). Both *Gsdme*$^{+/+}$ and *Gsdme*$^{-/-}$ EMT6 tumours grew more rapidly in NSG than in wild-type mice, indicating immune protection in the wild-type mice even in the absence of GSDME. *Gsdme* deficiency did not markedly affect tumour growth in NSG mice, whereas *Gsdme*$^{-/-}$ EMT6 tumours grew faster in immunocompetent mice. A requirement for lymphocytes in the anti-tumour effect of GSDME was also observed by comparing empty-vector and mGSDME-overexpressing B16 tumours (Fig. 2c). To determine whether killer cells are important for GSDME-mediated tumour inhibition, we implanted *Gsdme*$^{+/+}$ and *Gsdme*$^{-/-}$ EMT6 tumours in mice lacking CD8$^+$ T cells and/or NK cells and in mice treated with control antibodies (Fig. 2b and Extended Data Fig. 7). Depletion of either CD8$^+$ T or NK cells modestly but noticeably reduced GSDME-mediated tumour inhibition, but GSDME expression did not alter tumour growth substantially in mice lacking both CD8$^+$ T and NK cells, indicating that both types of killer cell are responsible for tumour suppression (Fig. 2b). Similarly, depletion of either killer-cell subset markedly increased the growth of only GSDME-expressing and not empty-vector B16 cells (Extended Data Fig. 8). Thus, both CD8$^+$ T and NK cells mediate the tumour-suppressive effects of GSDME.

This killer-cell dependence of protection suggests that pyroptosis causes immunogenic cell death (ICD)[9]. The gold-standard criterion of ICD is protection from secondary-tumour challenge after vaccination with tumour cells undergoing ICD. To determine whether pyroptosis causes ICD, we vaccinated mice with either wild-type or GSDME-overexpressing B16 cells subcutaneously in the left flank, and further challenged the mice ten days later with wild-type B16 on the right flank (Fig. 2d–f). At the vaccination site, GSDME and caspase 3 cleavage were easily detected by immunoblot only in GSDME-overexpressing tumours (Fig. 2d), indicating that pyroptosis occurred spontaneously in vivo and that cell death increased greatly in GSDME-overexpressing tumours. Moreover, vaccination with GSDME-overexpressing, compared with wild-type, B16 cells substantially reduced the growth of challenge wild-type B16 tumours (Fig. 2e) and improved tumour-free survival (Fig. 2f). Five of eight mice vaccinated with wild-type B16 cells developed palpable tumours, whereas only one of eight mice vaccinated with GSDME-overexpressing B16 cells did ($P = 0.039$, χ^2 test). Thus, pyroptosis is a form of ICD that occurs spontaneously in GSDME-overexpressing tumours.

Recognition by CD8$^+$ T and NK cells triggers both cytokine secretion and cytotoxic granule-mediated, PFN-dependent cell killing, but the latter is generally considered key to anti-tumour immunity. To determine whether killing mediates tumour suppression, we compared the growth of empty-vector and mGSDME-overexpressing 4T1E tumours in wild-type and *Prf1*$^{-/-}$ (PFN-deficient) mice (Fig. 2g). Both tumours grew much faster in PFN-deficient than in wild-type mice. Although GSDME markedly reduced 4T1E growth in wild-type mice, GSDME conferred no noticeable advantage in PFN-deficient mice, indicating that granule-dependent cytotoxicity was responsible for GSDME's tumour suppression. Given that GSDME had no substantial effect on tumour growth in mice lacking killer lymphocytes or PFN, GSDME's tumour suppression

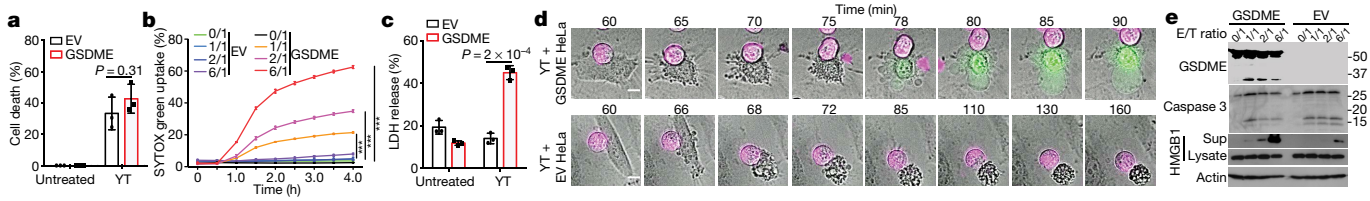

Fig. 3 | Killer cells cleave GSDME and induce GSDME-dependent pyroptosis in target cells. a–**c**, Death of empty vector and hGSDME-expressing HeLa cells induced by YT NK cells, assessed by CellTiter-Glo (**a**; effector cell/target cell (E/T) ratio = 2/1; 4 h), SYTOX green uptake (**b**, E/T ratios indicated) and LDH release (**c**, E/T ratio = 2/1; 4 h). **d**, Time-lapse confocal microscopy images of cocultures of Vybrant-DiD-labelled YT cells (magenta) with empty vector and hGSDME-positive HeLa cells in medium containing SYTOX green. **e**, Caspase 3 and GSDME cleavage and HMGB1 release in HeLa cells incubated with YT cells at the indicated E/T ratios for 4 h, assessed by immunoblot. Comparisons were calculated by two-tailed Student's *t*-test (**a**, **c**) or by one-way ANOVA with Holm–Sidak method for multiple comparisons (**b**). Data are mean ± s.d. of biological triplicates and are representative of three independent experiments. ***$P < 0.0001$. Scale bar, 10 µm.

must be primarily mediated by killer lymphocytes. GSDME-negative tumours tended to be larger than GSDME-positive tumours at later time points even in NSG and lymphocyte-depleted mice, suggesting that cell-intrinsic mechanisms of GSDME-mediated tumour suppression may exist.

Killer cells activate pyroptosis

The strong dependence of GSDME-mediated tumour suppression on cytotoxicity suggested that killer lymphocytes might cause pyroptosis in GSDME-expressing targets. To determine whether killer cells induce pyroptosis, we incubated the human NK line YT with empty-vector and hGSDME-overexpressing HeLa cells. Although cell death was comparable (Fig. 3a), pyroptosis occurred only in GSDME-expressing HeLa cells and increased with more NK cells (Fig. 3b, c). Using time-lapse microscopy, we found that both empty-vector and GSDME-positive HeLa cells began to detach about an hour after adding YT cells (Fig. 3d and Supplementary Videos 5, 6). Empty-vector HeLa cells showed progressive apoptotic morphology and did not take up SYTOX green over 160 min, whereas GSDME-positive HeLa cells began to take up SYTOX green after 15–20 min and underwent increasing pyroptotic membrane ballooning. Caspase 3 was cleaved in YT-cocultured empty-vector and GSDME-expressing HeLa cells collected 4 h after adding YT cells, but GSDME was cleaved only in GSDME-positive tumours, which released much more HMGB1 (Fig. 3e).

Treatment of GSDME-positive HeLa cells with YT cells or another human NK line, NK-92, or with raptinal or TRAIL produced a GSDME fragment of the same size (Fig. 4a), suggesting that NK cells cleaved GSDME at the caspase 3 site. To determine whether NK-cell-induced pyroptosis depends on cytotoxic granule release, we measured pyroptosis in the presence or absence of the Ca^{2+} chelator EGTA, which inhibits cytotoxic granule release and PFN (Fig. 4b). EGTA completely blocked pyroptosis, suggesting that degranulation was required. The caspase 3 inhibitor zDEVD-fmk or the pan-caspase inhibitor zVAD-fmk only partially blocked YT-induced pyroptosis. To confirm caspase-3-independent pyroptosis, we compared YT-mediated killing of *CASP3*$^{+/+}$ and *CASP3*$^{-/-}$ hGSDME-overexpressing HeLa cells (Fig. 4c, d). We found that *CASP3* deficiency only partially reduced YT-induced pyroptosis, suggesting that NK cells activated both caspase-dependent and caspase-independent pyroptosis. To test whether necroptosis or ferroptosis—other caspase-independent inflammatory death pathways—contribute, we added a necroptosis inhibitor (necrostatin-1s; ref. [10]) or three ferroptosis inhibitors (ferrostatin-1, α-tocopherol or desferoxamine[11]), to YT cocultures with empty-vector or GSDME-overexpressing HeLa cells (Extended Data Fig. 9a). None of these inhibitors suppressed YT-induced pyroptosis of GSDME-overexpressing HeLa cells, suggesting that necroptosis and ferroptosis are not involved. Moreover, expression of receptor-interacting serine/threonine kinase 3 (*RIPK3*), a protein that is needed to activate necroptosis, was not detected by quantitative reverse transcription (qRT)–polymerase chain reaction (PCR) in any of the cell lines studied (Extended Data Fig. 9b–e). Thus, cytotoxic granule release induces partly caspase-independent pyroptosis in GSDME-positive tumours.

Granzyme B cleaves GSDME after D270

Because NK-induced pyroptosis in GSDME-expressing cells does not require caspases, we speculated that Gzm proteases might cleave GSDME. Gzm-mediated cell death is caspase-independent, but is amplified by caspases because GzmB cuts and activates caspase 3 (ref. [12]). To test whether Gzms cleave GSDME, we incubated lysates from hGSDME-overexpressing or hGSDMD-overexpressing HEK293T cells with purified human GzmA or GzmB, the most abundant Gzms. GzmB, but not GzmA, led to GSDME but not GSDMD cleavage (Fig. 4e). Given that the caspase-activated and killer-cell-activated GSDME N termini were of similar sizes (Fig. 4a), GzmB either activates caspase 3 to cleave GSDME and/or directly cleaves GSDME at the same residue. In fact, GzmB did not activate cleavage of the GSDME D270A mutant, but wild-type GSDME was still cleaved when all caspases were inhibited (Fig. 4f) or in lysates of *CASP3*$^{-/-}$ GSDME-overexpressing HeLa cells (Fig. 4g), suggesting that GzmB directly cleaves GSDME after D270. We verified this direct cleavage by showing that GzmB cleaved recombinant GSDME (Fig. 4h). To determine whether GzmB cleaves GSDME in cells, we treated SH-SY5Y, a GSDME-positive human neuroblastoma, with PFN with or without GzmB (Fig. 4i and Extended Data Fig. 10a–c). The combination, but not PFN alone, caused pyroptotic morphology (Extended Data Fig. 10a). Within 30 min of adding GzmB and PFN, GSDME and caspase 3 cleavage were detected by immunoblot (Fig. 4i). GSDME cleavage and LDH release from SH-SY5Y required GzmB and PFN, and were partially inhibited by inhibiting caspase 3 or all caspases (Extended Data Fig. 10b, c). Knocking out *GSDME* by CRISPR–Cas9 in SH-SY5Y (Extended Data Fig. 1h) did not change overall GzmB- and PFN-mediated cell death (Fig. 4j), but blocked pyroptosis (Fig. 4k and Extended Data Fig. 10d). Thus, GzmB induces GSDME-dependent pyroptosis in tumour targets both directly by cleaving GSDME and indirectly by activating caspase 3.

D270 cleavage mediates tumour suppression

Because both GzmB and caspase 3 use cleavage at D270 to activate GSDME, mutation of this residue in tumours should abrogate tumour suppression. To test this hypothesis, we compared the growth of B16 (Extended Data Fig. 11a–d) and 4T1E (Extended Data Fig. 11e–h) cells stably overexpressing wild-type or D270A mGSDME or empty vector. Although wild-type GSDME reduced tumour growth as before (Fig. 1

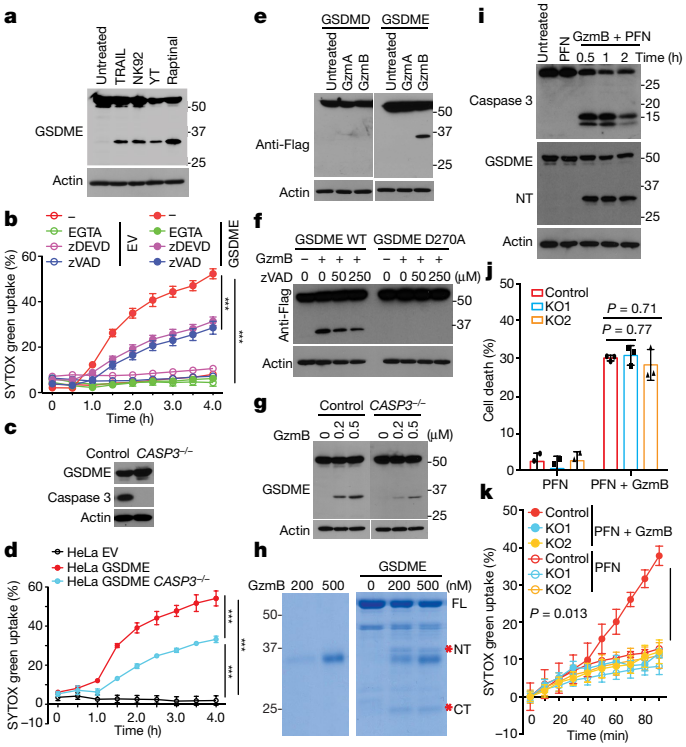

Fig. 4 | GzmB directly cleaves GSDME to cause pyroptosis. a, Immunoblot of hGSDME-positive HeLa cells after no treatment or treatment with YT or NK92 cells or with TRAIL for 4 h or raptinal for 1 h. **b**, Effect of EGTA, zVAD-fmk and zDEVD-fmk on YT-induced SYTOX green uptake in empty vector and hGSDME-positive HeLa cells. **c**, **d**, Expression of GSDME and caspase 3 in hGSDME-positive (control) and hGSDME-positive *CASP3*$^{-/-}$ HeLa cells (**c**) and YT-induced SYTOX green uptake (**d**) in empty vector and hGSDME-positive and hGSDME-negative *CASP3*$^{-/-}$ HeLa cells. **e**, **f**, Immunoblots, probed for Flag–GSDMD (**e**, left) or Flag–GSDME (**e**, right; **f**), of cell lysates of HEK293T cells expressing Flag-tagged wild-type or D270A (**f**, right lanes) hGSDME after 1 h incubation with phosphate-buffered saline (PBS) or recombinant GzmA or GzmB (800 nM). **g**, Immunoblots, probed for GSDME, of cell lysates of hGSDME-positive HeLa cells, knocked out or not (control) for *CASP3*, after 1 h incubation with GzmB. **h**, Coomassie-stained SDS–PAGE gel of in vitro reaction of recombinant GzmB incubated with recombinant hGSDME for 1 h. *NT and *CT, N-terminal and C-terminal GSDME cleavage products; FL, full-length GSDME. **i**, SH-SY5Y cells treated with PFN plus or minus GzmB or with medium ('Untreated'), for 2 h or for the indicated times, were analysed by immunoblot of cell lysates probed for caspase 3, GSDME or actin. **j**, **k**, Effects of *GSDME* knockout (KO) on the cell death and pyroptosis of SH-SY5Y cells treated with PFN plus or minus GzmB, assessed after 1 h by CellTiter-Glo (**j**) or SYTOX green uptake (**k**). Differences among multiple groups in **b**, **d**, **j**, **k** were analysed by one-way ANOVA using the Holm–Sidak method for multiple comparisons. Data are mean ± s.d. of biological triplicates and are representative of three (**a**–**h**) or two (**i**–**k**) independent experiments. ***$P < 0.0001$.

and Extended Data Fig. 6), tumours overexpressing D270A GSDME or expressing empty vector grew indistinguishably (Extended Data Fig. 11a, e). Overexpression of wild-type GSDME enhanced CD8$^+$ and NK TIL functionality, but overexpression of D270A GSDME did not alter GzmB, PFN or cytokine expression in CD8$^+$ or NK TILs (Extended Data Fig. 11b–d, f–h). When *Gsdme*$^{-/-}$ EMT6 cells were knocked in to express empty vector or wild-type, F2A nonfunctional or D270A noncleavable GSDME at levels comparable to that of endogenous GSDME in wild-type EMT6, only wild-type GSDME substantially reduced tumour growth (Extended Data Fig. 11i, j), providing additional evidence that GSDME cleavage at D270 and pore formation are required for tumour suppression.

Discussion

Here we have shown in melanoma, triple negative breast cancer and colorectal cancer tumours that GSDME expression acts as a tumour suppressor by inducing pyroptosis, which enhances anti-tumour killer-cell cytotoxicity. The anti-tumour activity of GSDME was abrogated in mice lacking killer lymphocytes or PFN. Mutations abolishing GSDME pore formation or cleavage by GzmB/caspase 3 also blocked tumour suppression. Tumour suppression occurred without any extrinsic treatment. We consider what it is that initially triggers in vivo pyroptosis. It may have been initiated by spontaneous apoptosis of hypoxic or stressed regions of the tumour or by immune-mediated killing. Our working model is that GSDME expression in spontaneously dying tumour cells provides inflammatory danger signals that recruit immune cells to the tumour microenvironment and promote their functionality. GSDME expression increased not only the number and function of TILs, but also macrophage-mediated phagocytosis, which is predicted to enhance anti-tumour adaptive immunity. Some tumours evade immunity by resisting phagocytosis[13,14]; tumour GSDME may help to overcome this immune evasion strategy.

Killer-cell-mediated death was previously thought of as noninflammatory. Here we have shown, however, that killer lymphocytes activate pyroptosis when GzmB cleaves GSDME at the caspase 3 site. Caspase-resistant cancer cells should be susceptible to killer-cell-mediated apoptosis (because Gzm-activated death is mostly caspase-independent) as well as pyroptosis, provided that the cancer cells express GSDME. Pyroptosis may augment killer-cell immunity by providing adjuvant-like danger signals. Our results indicate that pyroptosis, similar to necroptosis[15], is a form of ICD[9]. Implanted GSDME-positive B16 melanoma cells, but not GSDME-negative cells, spontaneously underwent pyroptosis and protected mice from challenge with wild-type B16 cells. Protection by such vaccination—the gold standard for ICD[9]—did not require chemotherapy or radiation, suggesting that GSDME-expressing tumours, even otherwise 'immunologically cold' tumours such as B16, are spontaneously undergoing pyroptotic ICD in vivo. It is worth noting that the GSDME-positive tumours studied here do not release interleukin (IL)-1β or require it for immune protection, because *Il1b* was expressed by only one of the mouse cell lines studied (Extended Data Fig. 9f, g) and IL-1β was not detected in sera of GSDME-positive tumour-bearing mice (data not shown).

Direct Gzm-mediated induction of pyroptosis provides a simple mechanism for triggering inflammatory death—much simpler than canonical inflammasome activation, which requires at least four molecules (a sensor, an adaptor, an inflammatory caspase and GSDMD), or even the noncanonical pathway, which requires an inflammatory caspase and GSDMD. GSDME and other GSDMs may sense other mislocalized cytosolic proteases as danger signals. The GSDM linker region is an unstructured loop, making it a good protease substrate. Consistent with this, neutrophil serine proteases, which are homologous to Gzms, can cleave GSDMD to induce neutrophil netosis[16,17].

Cancer cells have developed two strategies—epigenetic suppression of *GSDME* expression and LOF mutations—to avoid GSDME-mediated tumour suppression. Epigenetic suppression of *GSDME* is more common than *GSDME* mutation[2,4,6]. We have shown here that many cancer-related *GSDME* mutations reduce pyroptosis, and that mutations of D270, the shared GzmB/caspase 3 cleavage site and a prominent cancer mutation, have enabled tumours to evade tumour suppression by GSDME. Therapeutic strategies to induce *GSDME*—such as use of the DNA methylation inhibitor decitabine[4], an approved leukaemia and myelodysplasia drug—are worth exploring.

Online content

Any methods, additional references, Nature Research reporting summaries, source data, extended data, supplementary information,

acknowledgements, peer review information; details of author contributions and competing interests; and statements of data and code availability are available at https://doi.org/10.1038/s41586-020-2071-9.

1. Liu, X. & Lieberman, J. A mechanistic understanding of pyroptosis: the fiery death triggered by invasive infection. *Adv. Immunol*. **135**, 81–117 (2017).
2. de Beeck, K. O., Van Laer, L. & Van Camp, G. DFNA5, a gene involved in hearing loss and cancer: a review. *Ann. Otol. Rhinol. Laryngol*. **121**, 197–207 (2012).
3. Rogers, C. et al. Cleavage of DFNA5 by caspase-3 during apoptosis mediates progression to secondary necrotic/pyroptotic cell death. *Nat. Commun*. **8**, 14128 (2017).
4. Wang, Y. et al. Chemotherapy drugs induce pyroptosis through caspase-3 cleavage of a gasdermin. *Nature***547**, 99–103 (2017).
5. Rogers, C. *et al*. Gasdermin pores permeabilize mitochondria to augment caspase-3 activation during apoptosis and inflammasome activation. *Nat. Commun*. **10**, 1689 (2019).
6. Xia, X. et al. The role of pyroptosis in cancer: pro-cancer or pro-"host"? *Cell Death Dis*. **10**, 650 (2019).
7. Palchaudhuri, R. et al. A small molecule that induces intrinsic pathway apoptosis with unparalleled speed. *Cell Reports***13**, 2027–2036 (2015).
8. Ruan, J., Xia, S., Liu, X., Lieberman, J. & Wu, H. Cryo-EM structure of the gasdermin A3 membrane pore. *Nature***557**, 62–67 (2018).
9. Galluzzi, L., Buqué, A., Kepp, O., Zitvogel, L. & Kroemer, G. Immunogenic cell death in cancer and infectious disease. *Nat. Rev. Immunol*. **17**, 97–111 (2017).
10. Teng, X. et al. Structure-activity relationship study of novel necroptosis inhibitors. *Bioorg. Med. Chem. Lett*. **15**, 5039–5044 (2005).
11. Wenzel, S. E. et al. PEBP1 wardens ferroptosis by enabling lipoxygenase generation of lipid death signals. *Cell***171**, 628–641 (2017).
12. Chowdhury, D. & Lieberman, J. Death by a thousand cuts: granzyme pathways of programmed cell death. *Annu. Rev. Immunol*. **26**, 389–420 (2008).
13. Nagata, S. Apoptosis and clearance of apoptotic cells. *Annu. Rev. Immunol*. **36**, 489–517 (2018).
14. Werfel, T. A. & Cook, R. S. Efferocytosis in the tumor microenvironment. *Semin. Immunopathol*. **40**, 545–554 (2018).
15. Aaes, T. L. et al. Vaccination with necroptotic cancer cells induces efficient anti-tumor immunity. *Cell Reports***15**, 274–287 (2016).
16. Sollberger, G. et al. Gasdermin D plays a vital role in the generation of neutrophil extracellular traps. *Sci. Immunol*. **3**, eaar6689 (2018).
17. Kambara, H. et al. Gasdermin D exerts anti-inflammatory effects by promoting neutrophil death. *Cell Reports***22**, 2924–2936 (2018).

Methods

Data reporting

No statistical methods were used to predetermine sample size. The experiments were not randomized and the investigators were not blinded to outcome assessment.

Cell lines and cell culture conditions

HeLa, HEK293T and EMT6 cells were purchased from ATCC. 4T1E and 4T1E–eGFP cells were generated in our laboratory by sorting 4T1 cells for high E-cadherin expression, as previously reported[18]. 4T1 and 4TO7 cells were gifts from F. Miller. B16F10 and CT26 cells were provided by G. J. Freeman. SH-SY5Y cells were a gift from Y. Shi. The YT-Indy NK cell line was a gift from Z. Brahmi. HeLa, HEK293T, 4T1, 4TO7, 4T1E, 4T1E GFP and B16F10 cells were cultured in Dulbecco's modified Eagle medium (DMEM) supplemented with 10% heat-inactivated fetal bovine serum (FBS), 6 mM HEPES, 1.6 mM L-glutamine, 50 μM 2-mercaptoethanol, 100 U ml^{-1} penicillin G and 100 μg ml^{-1} streptomycin sulfate. EMT6, CT26, SH-SY5Y and YT-Indy NK cells were cultured in RPMI medium with 10% FBS and the same supplements. All cells were verified to be free of mycoplasma by PCR and were authenticated by morphology only.

Plasmids

Full-length human *GSDMD* and *GSDME* and mouse *Gsdme* were cloned into pFlag-CMV4 plasmids. *GSDME* and *Gsdme* point mutation plasmids were generated by quick-change PCR (Stratagene). *GSDME* truncations were amplified by PCR from pFlag-CMV4-*GSDME*. pLVX-Puro empty vector was a gift from C. Bowman-Colin. Full-length wild-type *GSDME* and mutant *GSDME*s were cloned into pLVX-Puro using a Hifi one-step kit (Gibson Assembly). LentiCRISPR-v2 puro and LentiCRISPR-v2 hygro vectors were obtained from Addgene and guide RNAs were cloned into the vectors as previously described[19,20]. All plasmids were verified by sequencing.

Stable cell lines

To generate lentiviruses, pLVX-puro *Gsdme* plasmid was transfected into HEK293T cells with pSPAX2 and pCMV-VSV-G at a 1/1/2 ratio. Supernatants collected 2 days later were used to transduce B16 and 4T1E cells for 48 h. Puromycin (Sigma, 3 μg ml^{-1}) was then added to select GSDME-expressing cells. pLVX-puro *GSDME* was used to generate HeLa cells stably expressing *GSDME*, and pLVX-puro empty vector was used to generate control cells.

CRISPR–Cas9 knockout cells

Gsdme gRNAs (5′-TTTCTTAAAGAAGTTGATGC-3′ and 5′-CAAG CTGCAACTTCTAAGTC-3′) and *GSDME* gRNAs (5′-TAAGTTACAG CTTCTAAGTC-3′ and 5′-TGACAAAAAAGAAGAGATTC-3′) were cloned into LentiCRISPR-v2 puro, and *Casp3* gRNA (5′-GGAGAACACTG AAAACTCAG-3′) was cloned into LentiCRISPR-v2 hygro, as previously described[19,20]. The resulting plasmids were transfected into HEK293T cells with pSPAX2 and pCMV-VSV-G at a 1/1/2 ratio. Supernatants from HEK293T cells transfected with plasmids that express mouse *Gsdme*, human *GSDME* or *CASP3* guide RNAs were collected 2 days later and used to transduce mouse EMT6 and CT26 cell lines, human SH-SY5Y cells or GSDME-positive HeLa cells, respectively. Two days later, 3 μg ml^{-1} (8 μg ml^{-1} for CT26 cells) of puromycin or 200 μg ml^{-1} hygromycin was added to select for positive cells for 5 days or 14 days, respectively. Cells were then subcloned into 96-well plates and screened for GSDME expression by immunoblot. Selected knockout clones were analysed and verified by DNA sequencing. LentiCRISPR-v2 empty vector was used to generate control cells.

Reagents

Raptinal, EGTA, necrostatin-1s (Nec-1s), ferrostatin-1 (Fer-1), α-tocopherol (vitamin E) and desferoxamine (DFO) were from Sigma. TRIzol was from Life Technologies. TRAIL was from Enzo Life Sciences. zVAD-fmk and zDEVD-fmk were from BD Biosciences. SYTOX green was from Invitrogen. Vybrant DiD dye was from ThermoFisher Scientific. A CellTiter 96 kit (Promega) was used to measure cell proliferation.

Gene-expression assays

RNA was extracted using TRIzol reagent according to the manufacturer's instructions and was subject to reverse transcription using the SuperScript III system (Invitrogen). *Gsdme* expression was assayed by qRT–PCR using SsoFast Supermix (Bio-Rad). Breast cancer (BRCA) and colon cancer (COAD) RNA-sequence expression data were obtained from TCGA using the University of California Santa Cruz (UCSC) Xena bioinformatic tool[21]. The log2 difference between *GSDME* and *GAPDH* expression was calculated for both tumour and normal tissue and plotted using Prism software.

Immunoblot

Cells were lysed in lysis buffer (50 mM Tris-Cl pH 7.4, 150 mM NaCl, 1% Triton-X100 supplemented with 1 mM phenylmethylsulfonyl fluoride (PMSF) before use). Cell lysate in SDS loading buffer (50 mM Tris-HCl pH 6.8, 10% glycerol, 2% SDS, 1% 2-mercaptoethanol, 0.1% bromophenol blue) was boiled and analysed by SDS–PAGE (Bio-Rad) and transfer to polyvinylidene fluoride (PVDF) membranes (MilliporeSigma), which were then blocked with 2% milk in TBST buffer (150 mM NaCl, 20 mM Tris-HCl pH 7.6, 0.1% Tween-20) for 30 min before incubation with primary antibodies for 2 h at room temperature or 4 °C overnight. After washing with TBST, membranes were incubated with secondary antibody for 40 min and then washed three times with TBST before adding the West Femto substrate (ThermoFisher Scientific) for detection. Antibodies were anti-GSDME (ab215191, Abcam), anti-Flag (F1804, Sigma), anti-caspase 3 (9662S, Cell Signaling), anti-HMGB1 (ab18256, Abcam), anti-α-tubulin (T5168, Sigma), and anti-β-actin (JLA20, Developmental Studies Hybridoma Bank).

Cell-death assays

To measure membrane lysis, culture medium was collected and LDH release was measured using the CytoTox 96 cytotoxicity assay (Promega) according to the manufacturer's instructions. To assess pyroptosis induced by the GSDME N terminus in HEK293T cells, we carried out HEK293T transfection using the calcium-phosphate method and measured LDH release 20 h after transfection. Pyroptotic cells were also imaged using an Olympus IX70 inverted microscope, and protein expression was analysed by immunoblot. For raptinal-induced pyroptosis in B16 GSDME cells, 10 μM raptinal was used to treat B16 cells for 2 h and LDH release was measured at indicated time points. For TRAIL-induced pyroptosis in HeLa GSDME cells, LDH release was measured 16 h after cells were treated with 100 ng ml^{-1} TRAIL. For YT-induced pyroptosis in HeLa GSDME cells, LDH release was measured 4 h after treatment (E/T ratio = 2/1). For PFN/GzmB-induced pyroptosis in SH-SY5Y cells, LDH was measured 1 h after treatment in GSDME-knockout cells or 2 h after treatment in the presence of caspase inhibitors.

Overall cell death due to pyroptosis or apoptosis was measured at the same time as LDH release. To measure overall cell death in raptinal-treated B16 cells, we stained samples with allophycocyanin (APC)-conjugated annexin V (Invitrogen) and propidium iodide (PI) (Sigma) according to the manufacturer's instructions and analysed the results by BD FACSCanto II (BD Biosciences) using FlowJo V.10 (TreeStar) software. Cell death was determined by counting annexin V and/or PI-positive cells. To measure overall cell death in HeLa or SH-SY5Y cells, we assessed cell viability by measuring ATP levels using a CellTiter-Glo kit (Promega). The untreated cells were considered as a 100% viability control and cell death was inferred as a reduction in the number of viable cells.

SYTOX green uptake and time-lapse microscopy

To assess raptinal-induced cell death, we seeded cells in 96-well plates overnight and treated them with 10 μM raptinal for 2 h in the presence of

2.5 μM SYTOX green. Fluorescence at 528 nM after excitation at 485 nM was continually recorded every 10 min using a Biotek Synergy plate reader. For time-lapse microscopy, cells seeded in glass-bottom 35-mm dishes (MatTek) overnight were treated with 10 μM raptinal in complete RPMI medium containing 2.5 μM SYTOX green and imaged using a Zeiss 880 laser scanning confocal microscope within an environmental chamber maintained at 37 °C and 5% CO_2.

For YT-induced cell death, HeLa cells were seeded in 96-well plates overnight and pretreated with EGTA (2 mM), zVAD-fmk (30 μM), zDEVD-fmk (30 μM), Nec-1s (20 μM), α-tocopherol (vitamin E, 100 μM), Fer-1 (2 μM) or DFO (100 μM) as indicated for 0.5 h, before YT cells at indicated E/T ratios and 2.5 μM SYTOX green were added. Fluorescence at 528 nM after excitation at 485 nM was continually recorded every 30 min using a Biotek Synergy plate reader. Readings were normalized to control wells containing only YT cells. For time-lapse microscopy, HeLa cells were seeded in glass-bottom 35-mm dishes overnight. YT cells, stained with Vybrant DiD dye according to the manufacturer's instructions, were added at an E/T ratio of 2/1 together with 2.5 μM SYTOX green. Beginning 1 h later, cells were visualized over 90 min in an environmental chamber using a Zeiss 880 laser scanning confocal microscope.

Mouse studies

All procedures were conducted in compliance with all the relevant ethical regulations and were approved by the Harvard Medical School Institutional Animal Care and Use Committee. Female C57BL/6, BALB/c and NOD.Cg-Prkdc^{scid} Il2rg^{tm1Wjl}/SzJ (NSG) mice (6–8 weeks old) were purchased from Jackson Laboratories. *Prf1*$^{-/-}$ mice (Jackson Laboratories) in the BALB/c background were bred on site. All mice were housed in the Harvard Medical School Animal Facility. For tumour-challenge experiments, B16 EV, B16 mGSDME and B16 mGSDME F2A cells (approximately 1.5×10^5 cells per mouse) or CT26 control and *Gsdme*$^{-/-}$ cells (approximately 2×10^6 cells per mouse) were injected subcutaneously into the right flank of C57BL/6 and BALB/c mice, respectively. 4T1E (empty vector, mGSDME, mGSDME F2A, mGSDME P212L or mGSDME D270A) cells (approximately 5×10^4 cells per mouse); 4T1E–eGFP empty vector and GSDME-overexpressing cells (approximately 1.5×10^5 cells per mouse); or EMT6 (control, *Gsdme*$^{-/-}$, *Gsdme*$^{-/-}$ knocked in to express empty vector, GSDME F2A, GSDME D270A, or wild-type GSDME) cells (approximately 3×10^5 cells per mouse) were injected into the fourth mammary fat pad of BALB/c mice. For the vaccine/challenge experiment, C57BL/6 mice were vaccinated with 1.5×10^5 B16 empty vector or B16 mGSDME cells in the left flank and challenged 10 days later with 2×10^5 B16 empty vector cells in the right flank. Tumour growth was monitored by measuring the perpendicular diameters of tumours every other day. When control tumours grew to roughly 3–4 mm in diameter (10–20 days after implantation), all mice in an experiment were killed and tumours were collected for analysis. For cell depletion in the B16 tumour model, CD8 antibody (clone 2.43), NK1.1 antibody (clone PK136) or the isotype control antibody (all from BioXCell) were injected intraperitoneally (300 μg per mouse) starting on day 2 after tumour challenge for three consecutive days, and every five days thereafter. For cell depletion in the EMT6 tumour model, NK cells were depleted with anti-asialo-GM1 antibody (30 μl per mouse, clone poly21460, BioLegend) on days −1, +1 and +6 of tumour challenge. Specific cell depletion was verified by staining for CD4, CD8, CD49b and NKp46, and by flow cytometry of peripheral blood mononuclear cells obtained on day 3 or 7 after tumour challenge and of tumour-infiltrating lymphocytes obtained at the time of necropsy (Extended Data Fig. 7a).

Isolation of tumour-infiltrating immune cells

Tumours were collected, cut into small pieces and treated with 2 mg ml^{-1} collagenase D, 100 μg ml^{-1} DNase I (both from Sigma) and 2% FBS in RPMI with agitation for 30 min. Tumour fragments were homogenized and filtered through 70-μm strainers, and immune cells were purified by Percoll-gradient centrifugation and washed with Leibovitz's L-15 medium.

Antibody staining and flow cytometry

To detect eGFP-tetramer-specific CD8$^+$ TILs, we stained cells with phycoerythrin-labelled eGFP-specific MHC class I (H-2K^d) tetramer carrying the peptide HYLSTQSAL[22] (NIAID Tetramer Facility). Immune cells isolated from tumours were stained with CD45-PerCPCy5.5 (clone 30-F11), CD8-PacBlue, -PerCPCy5.5, -Alexa700, -fluorescein isothiocyanate (FITC) or -APC (clone 53-6.7), CD4-PE-Cy7, -APC or -PerCPCy5.5 (clone GK 1.5), CD49b-FITC, -PacBlue or -PerCPCy5.5 (clone DX5), NKp46-APC (clone 29A1.4), CD11b-Alexa700 (clone M1170), F4/80-PE-Cy7 (clone BM8) and CD44- PerCPCy5.5 (clone IM7) (BioLegend). Dead cells were excluded using the Aqua dead-cell stain kit (ThermoFisher Scientific) added with cell-surface antibodies. For intracellular staining, cells were first stained with antibodies to cell-surface markers for 30 min, then fixed and permeabilized with fixation/permeabilization buffer (BD Pharmingen) and stained with GzmB-PacBlue (clone GB11, ThermoFisher Scientific) and perforin-phycoerythrin (clone S16009B, BioLegend). For intracellular cytokine staining (ICS), roughly 10^6 cells per sample were cultured in RPMI medium containing 2% FBS and stimulated with either PMA (50 ng ml^{-1}, Sigma), ionomycin (2 μg ml^{-1}, Sigma) and Golgiplug (1.5 μl ml^{-1}, ThermoFisher Scientific) for 4 h, or with $eGFP_{200–208}$ (HYLSTQSAL peptide; 10 μg ml^{-1}, Genscript) and Golgiplug for 6 h. Cells were then stained with IFNγ-PacBlue (clone XMG1.2) and TNF-phycoerythrin-Cy7 (clone MP6-XT22) after fixation/permeabilization.

Protein expression and purification

The full-length coding sequence of human *GSDME* was cloned into the pDB.His.MBP vector to generate a recombinant construct with an N-terminal polyhistidine–maltose-binding protein (His_6–MBP) tag followed by a tobacco etch virus protease (TEV) cleavage site. The plasmid was verified by DNA sequencing and transformed into *Eschericha coli* BL21 (DE3) cells. Successful transformants were selected on an LB plate supplemented with 50 μg ml^{-1} kanamycin, transferred to LB medium with the same antibiotic, and grown at 37 °C with vigorous shaking until the optical density reached 1.0. Protein expression was then induced with 0.5 mM isopropyl-β-D-thiogalactopyranoside (IPTG) at 26 °C overnight. Cells were collected by centrifugation and frozen in liquid nitrogen for long-term storage at −80 °C. To purify human GSDME, we resuspended thawed *E. coli* pellets in buffer A (50 mM Tris-HCl at pH 8.0, 150 mM NaCl) and sonicated the cells to lyse them. The recombinant protein was captured on nickel-charged (Ni)-NTA beads (Qiagen) using a gravity-flow column and eluted with buffer A supplemented with 500 mM imidazole. The His_6–MBP tag was removed by overnight incubation with TEV at 4 °C followed by Ni-NTA affinity chromatography. The flow-through containing GSDME was concentrated and further fractionated using a Superdex 200 gel filtration column (GE Healthcare Life Sciences) equilibrated with buffer A. Monomer fractions of GSDME were pooled and frozen at −80 °C for further use.

Recombinant GzmA and GzmB were purified from HEK293T cells and PFN was purified from YT-Indy NK cells as previously described[23,24].

PFN/GzmB killing assay

The PFN/GzmB-mediated killing assay in SH-SY5Y cells was performed as previously described[24]. In brief, 500 nM GzmB and/or sublytic PFN in buffer P (10 mM HEPES pH 7.5 in Hanks' balanced salt solution (HBSS)) was added to SH-SY5Y cells in buffer C (10 mM HEPES pH 7.5, 4 mM $CaCl_2$, 0.4% bovine serum albumin (BSA) in HBSS). The sublytic concentration of PFN was determined as a concentration that caused 5–15% cytolysis of the target cell on its own. After 2 h incubation, LDH release, cell death, SYTOX green uptake and GSDME cleavage were assayed as described above.

In vitro cleavage assay

For in vitro cleavage in cell lysates, HEK293T cells transiently expressing Flag–hGSDMD or Flag–hGSDME for 48 h were lysed in lysis buffer containing 50 mM Tris-HCl pH 7.4, 150 mM NaCl and 1% Triton X100 (2×10^6 cells per millilitre), and cell lysates (20 µl) were incubated with GzmA or GzmB at 37 °C for 1 h. Cleavage products were detected by anti-Flag immunoblot. Cleavage of recombinant GSDME protein by recombinant GzmB was analysed by SDS–PAGE and Coomassie staining after incubation in buffer A at 37 °C for 1 h.

Statistics

A Student's *t*-test (two-tailed) or Mann–Whitney test was used to determine differences between two groups. Multiple comparisons between two groups were performed by multiple *t*-test with type I error correction. One- or two-way ANOVA was used to calculate differences among multiple populations. Differences between tumour growth curves and SYTOX green uptake curves were compared by first calculating the area-under-curve values for each sample and then comparing different groups using the Student's *t*-test or one-way ANOVA. Type I errors were corrected by the Holm–Sidak method. *P* values of less than 0.05 were considered significant.

Reporting summary

Further information on research design is available in the Nature Research Reporting Summary linked to this paper.

Data availability

All relevant data are available in the Source Data (for Figs. 1–4 and Extended Data Figs. 1–11) or Supplementary Information associated with this paper.

18. Petrocca, F. et al. A genome-wide siRNA screen identifies proteasome addiction as a vulnerability of basal-like triple-negative breast cancer cells. *Cancer Cell***24**, 182–196 (2013).
19. Shalem, O. et al. Genome-scale CRISPR-Cas9 knockout screening in human cells. *Science***343**, 84–87 (2014).
20. Sanjana, N. E., Shalem, O. & Zhang, F. Improved vectors and genome-wide libraries for CRISPR screening. *Nat. Methods***11**, 783–784 (2014).
21. Goldman, M. et al. The UCSC Xena platform for public and private cancer genomics data visualization and interpretation. Preprint at https://www.biorxiv.org/content/10.1101/326470v6 (2019).
22. Gambotto, A. et al. Immunogenicity of enhanced green fluorescent protein (EGFP) in BALB/c mice: identification of an H2-Kd-restricted CTL epitope. *Gene Ther*. **7**, 2036–2040 (2000).
23. Dotiwala, F. et al. A high yield and cost-efficient expression system of human granzymes in mammalian cells. *J. Vis. Exp*. **100**, e52911 (2015).
24. Thiery, J., Walch, M., Jensen, D. K., Martinvalet, D. & Lieberman, J. Isolation of cytotoxic T cell and NK granules and purification of their effector proteins. *Curr. Prot. Cell Biol*. **40**, 3.37.1–3.37.40 (2010).

Acknowledgements We thank the US National Institutes of Health (NIH) Tetramer Core Facility for providing the eGFP tetramer. This work was supported by NIH grant R01 AI139914 (to H.W. and J.L.), a Charles A. King Trust Fellowship (to Z.Z.) and a Department of Defense Breast Cancer Breakthrough Fellowship Award (to Y.Z.). The mutations in GSDME primary tumours and primary human breast cancer and colorectal cancer expression analyses in this study are based upon data generated by The Cancer Genome Atlas (TCGA) Research Network (https://www.cancer.gov/tcga).

Author contributions Z.Z. conceived the study. Z.Z., Y.Z. and J.L. designed experiments and analysed data. Z.Z. and Y.Z. performed the majority of the experiments, assisted by S.X., Q.K., S.L., X.L., C.J., K.F.M.-S., T.M.Y.M. and J.A. S.S., Y.Y. and H.W. analysed the locations of GSDME mutations, helped to prepare recombinant proteins and provided valuable comments. J.L., Z.Z. and Y.Z. wrote the manuscript.

Competing interests The authors declare no competing interests.

Additional information

Supplementary information is available for this paper at https://doi.org/10.1038/s41586-020-2071-9.

Correspondence and requests for materials should be addressed to Z.Z. or J.L.

Peer review information*Nature* thanks Ed Mocarski, Dmitri V. Krysko and the other, anonymous, reviewer(s) for their contribution to the peer review of this work.

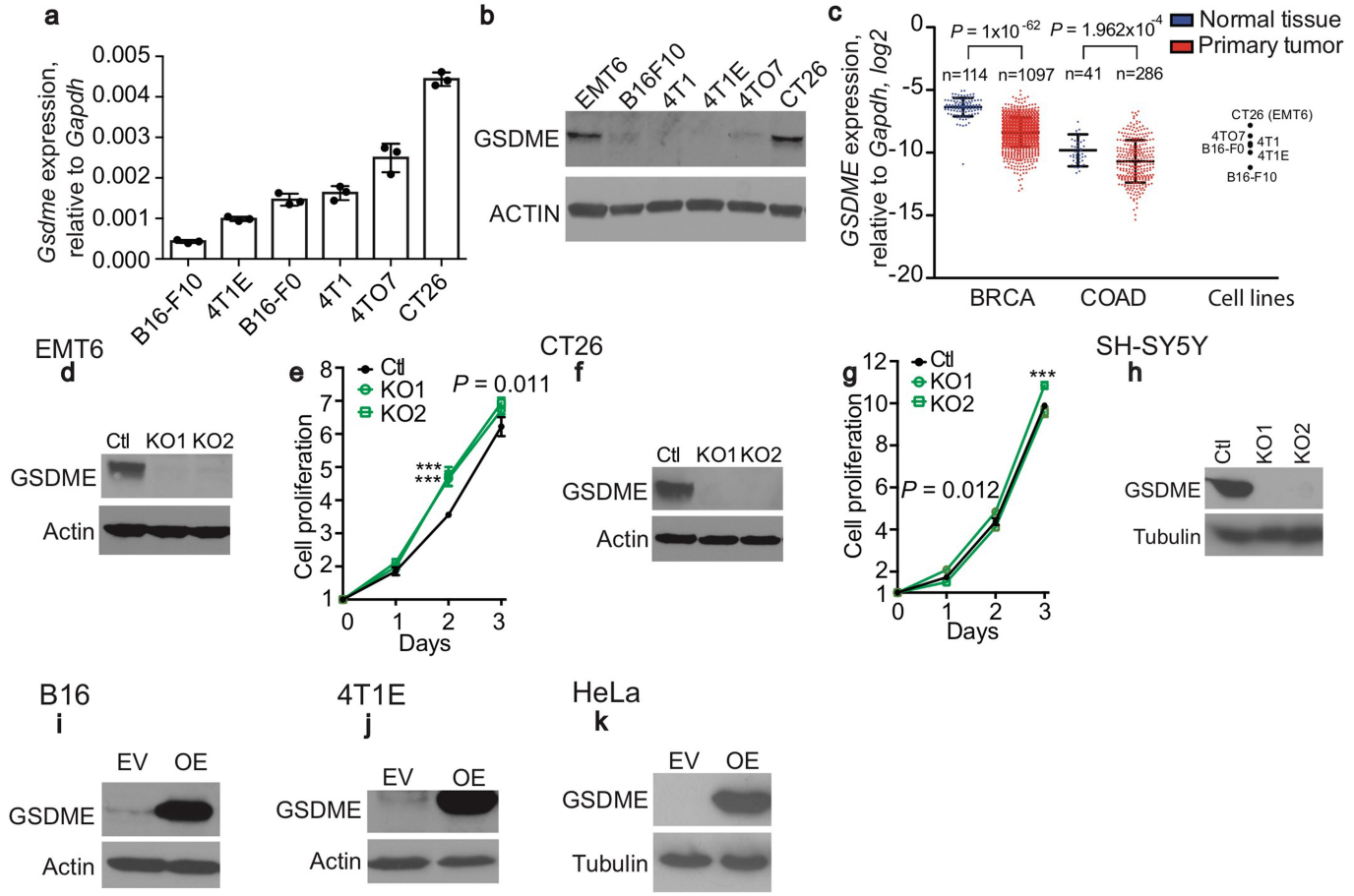

Extended Data Fig. 1 | GSDME expression in human and mouse tumour cell lines. a, **b**, *Gsdme* messenger RNA (**a**) and protein (**b**) levels in the indicated mouse cancer cell lines, assessed by qPCR, relative to *Gapdh* (**a**), and by immunoblot (**b**). **c**, *GSDME* expression relative to *GAPDH* in normal tissue and tumours from breast invasive carcinoma (BRCA) and colon adenocarcinoma (COAD) patients from TCGA, compared with the qRT–PCR values for mouse cancer cell lines used here. *P* values comparing normal tissue and cancer tissues were calculated using unpaired two-tailed Student's *t*-test. **d**, **f**, Expression of mGSDME in EMT6 (**d**) and CT26 (**f**) clones knocked out for *Gsdme*, or in control (Ctl) cells treated with nontargeting vector, assessed by immunoblot for GSDME. Actin serves as a loading control. **e**, **g**, Cell proliferation determined by CellTiter 96 in EMT6 (**e**) or CT26 (**g**) control and *Gsdme* knockout cells ($n = 6$ samples per group). **h**, Expression of hGSDME in SH-SY5Y clones knocked out for *GSDME* or in control cells treated with nontargeting vector, assessed by immunoblot for GSDME. **i**, **j**, Expression of mGSDME in GSDME-overexpressing (OE) and empty-vector-transduced B16 (**i**) or 4T1E (**j**) cells, assessed by immunoblot. **k**, Expression of hGSDME in GSDME-overexpressing and empty-vector-transduced HeLa cells, assessed by immunoblot. Differences among multiple groups in **e**, **g** were analysed by one-way ANOVA, using the Holm–Sidak method for multiple comparisons. *P* values in **e**, **g** compare knockout and control cells. ***$P < 0.0001$. Data are mean ± s.d. of three technical (**a**) or six biological (**e**, **g**) replicates. Data are representative of at least two independent experiments.

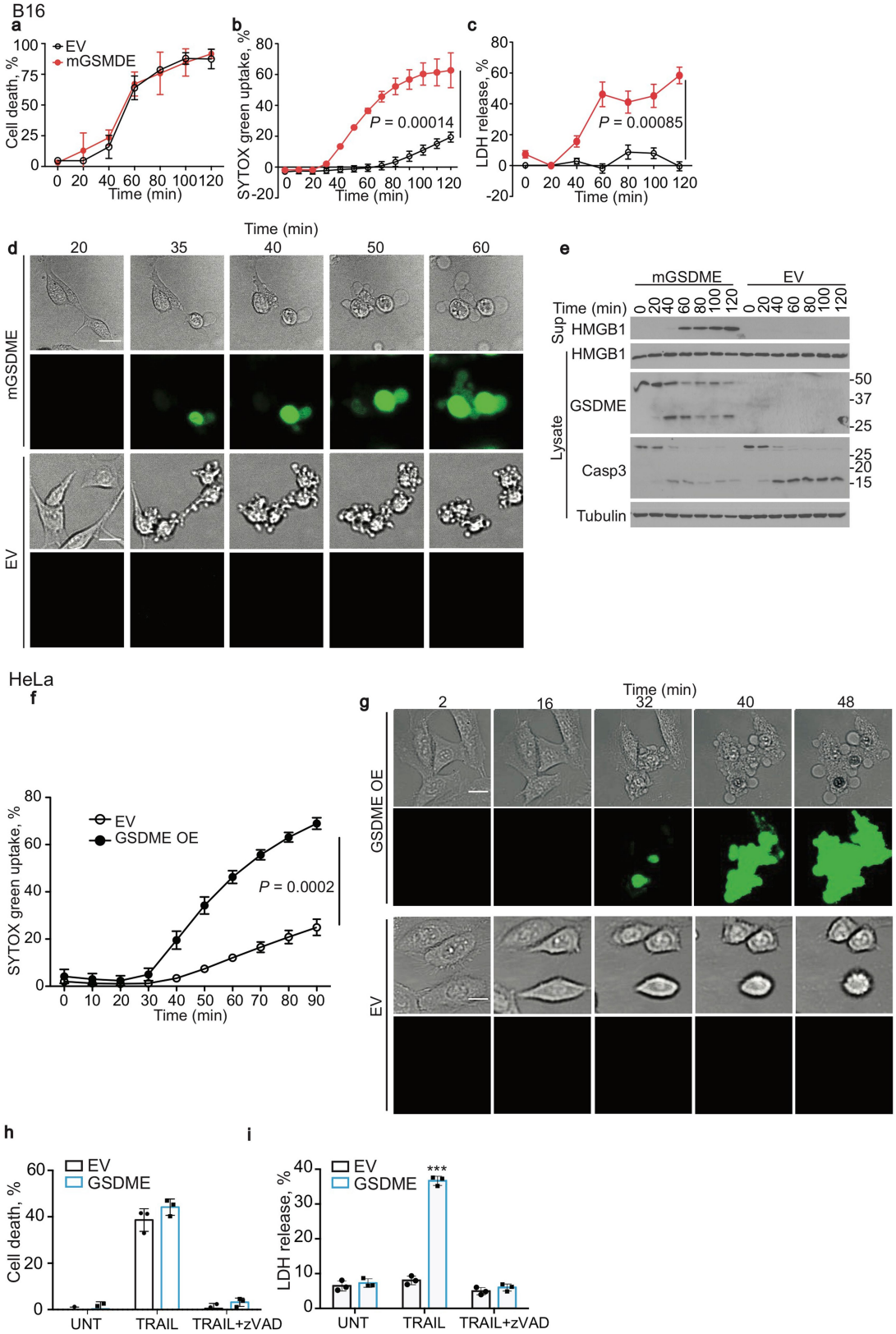

Extended Data Fig. 2 | See next page for caption.

Extended Data Fig. 2 | Raptinal and/or TRAIL induces pyroptosis in B16 and HeLa cells overexpressing GSDME. a–**e**, Comparison of cell death after adding raptinal to empty vector and mGSDME-overexpressing B16 cells. **a**, Kinetics of overall cell death, assayed by counting annexin-V-positive and/or PI-positive cells by flow cytometry. **b**, **c**, Pyroptosis assessed by SYTOX green uptake (**b**) and LDH release (**c**). **d**, Time-lapse microscopy images showing morphological changes and SYTOX green uptake. **e**, Kinetics of caspase 3 and GSDME cleavage and HMGB1 release by immunoblot of cell lysates and culture supernatants. **f**, **g**, SYTOX green uptake assessed by plate reader (**f**) and time-lapse confocal microscopy (**g**) after treatment of empty vector and hGSDME-overexpressing HeLa cells with raptinal. **h**, **i**, TRAIL-mediated induction of cell death at 16 h post treatment, assessed by CellTiter-Glo (**h**), and LDH release in HeLa cells transduced with an empty vector or in hGSDME-overexpressing HeLa cells in the presence or absence of the pan-caspase inhibitor zVAD-fmk (**i**). UNT, untreated. The areas under the curve in **a**–**c**, **f** and data in **h**, **i** were compared by two-tailed Student's *t*-test. Data are means ± s.d. of biological triplicate wells. ***$P < 0.0001$. Scale bar, 20 μm. Data are representative of two independent experiments.

a

Cancers	Mutations	Location	Significant amino acid change	Residue conserved
Adrenal gland adenomas and adenocarcinomas	L491*			
Breast carcinoma	D14Y	Globular, near subunit interface	Yes	Yes
	L118M	Transmembrane	No	Yes
	L451*			
Colon adenocarcinoma	D18V	Globular, near subunit interface	Yes	Yes
	N24D	Globular, near subunit interface	Yes	Yes
	V73M	Globular	No	No
	R108C	Transmembrane	Yes	No
	T196M	Transmembrane, near subunit interface	Yes	No
Gastric cancer adenocarcinoma	A3T	Globular, near subunit interface	No	No
	T6A	Globular	Yes	Yes
	L101P	Transmembrane	Yes	No
	E134A	Globular	Yes	Yes
Head and neck squamous cell carcinoma	L25V	Globular, near subunit interface	No	Yes
	G90V	Transmembrane, near subunit interface	No	Yes
	E177V	Transmembrane	Yes	No
	E233K	Globular	Yes	No
Liver cancer hepatocellular carcinoma	S75L	Globular	Yes	Yes
	M174V	Transmembrane	No	No
	N206K	Transmembrane, near subunit interface	Yes	No
	L236I	Globular	No	No
Lung cancer adenocarcinoma	W44C	Globular	Yes	Yes
	R108H	Transmembrane	Yes	No
	V109I	Transmembrane	No	Yes
	I129M	Globular	No	No
	E210*			
	I217N	Globular	Yes	Yes
Melanoma	L158F	Globular	No	Yes
	P212L	Between transmembrane and globular, near subunit interface	Yes	Yes
Ovarian cancer serous cystadenocarcinoma	K83N	Transmembrane, near subunit interface	Yes	Yes
	Q175E	Transmembrane	Yes	Yes
Renal cancer papillary carcinoma	I129N	Globular	Yes	No
Urothelial bladder cancer	S132C	Globular	Yes	No
Uterine corpus endometrioid carcinoma	G17D	Globular, near subunit interface	Yes	Yes
	L19M	Globular	No	Yes
	F43L	Globular	Yes	No
	W46*			
	R48I	Globular	Yes	Yes
	S55F	Globular, near subunit interface	Yes	No
	V88A	Transmembrane, near subunit interface	No	Yes
	E93K	Transmembrane, near subunit interface	Yes	No
	S107I	Transmembrane	Yes	No
	E134K	Globular	Yes	Yes
	I137T	Globular	Yes	Yes
	M174I	Transmembrane	No	No
	G199E	Transmembrane, near subunit interface	Yes	Yes
	G220S	Globular	Yes	No
	G239E	Globular	Yes	No

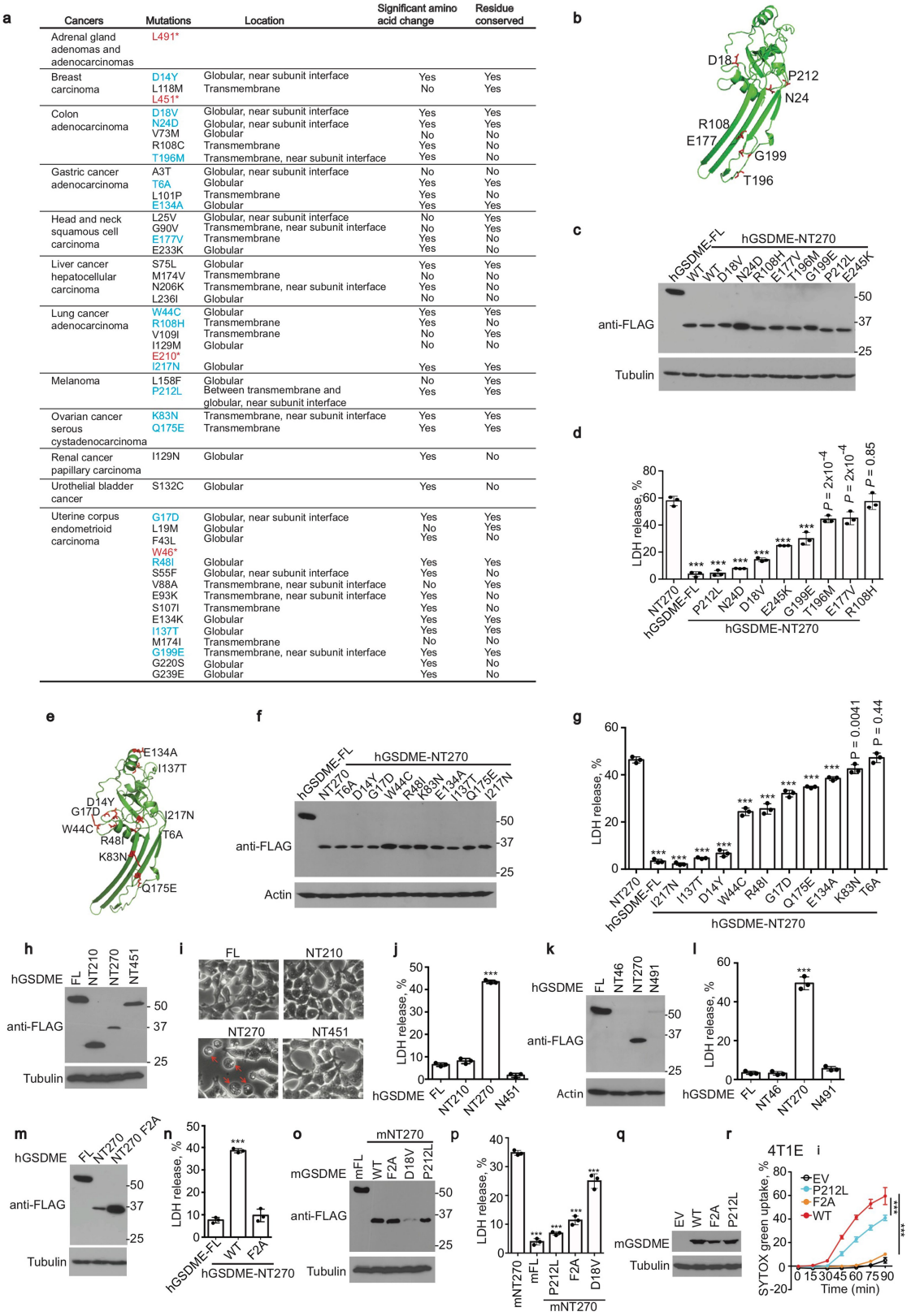

Extended Data Fig. 3 | See next page for caption.

Extended Data Fig. 3 | *GSDME* mutations in tumours are mostly LOF. **a**, GSDME N-terminal (NT) mutations in primary cancer cells in TCGA (https://www.cancer.gov/about-nci/organization/ccg/research/structural-genomics/tcga). Asterisks denote stop codons; red, truncations; blue, mutants analysed here. **b**–**g**, Seventeen GSDME-NT cancer-associated mutations are mapped onto GSDME-NT (amino acids 1–241)—modelled here on the basis of the cryo-electron microscopy structure of the pore conformation of the GSDMA3-NT (Protein DataBank identification code 6CB8)[8]. These mutations were analysed in two arbitrarily assigned groups (**b**, **e**). These 17 mutations and the E245K mutation were analysed, after transient expression of wild-type Flag-tagged GSDME (WT FL GSDME) or wild-type or mutated GSDME-NT (amino acids 1–270) in HEK293T cells, for GSDME expression by immunoblot (**c**, **f**) and for LDH release by CytoTox 96 assay (**d**, **g**). **h**–**l**, Effect of four cancer-related GSDME truncation mutations (resulting in shortened proteins comprising amino acids 1–46, 1–210, 1–451 and 1–491) on GSDME-mediated cell death. GSDME expression of truncated proteins or FL or GSDME-NT (1–270) in HEK293T cells (**h**, **k**) and their effect on HEK293T cell death, assessed by morphology using microscopy (**i**) and by LDH release (**j**, **l**). The NT46 truncated protein is too small to be detected in **k**. Red arrows indicate ballooning pyroptotic cells. **m**, **n**, Effect of F2A mutation on GSDME-NT-induced pyroptosis in HEK293T cells. Protein expression is detected by anti-Flag immunoblot (**m**) and pyroptosis is assessed by LDH release (**n**). **o**, **p**, Effect of transient expression of mouse WT FL GSDME or wild-type or mutated GSDME-NT (mNT270, amino acids 1–270) in HEK293T cells (**o**) and on LDH release (**p**). **q**, **r**, Effect in 4T1E cells of expression of wild-type or mutated FL mGSDME (**q**) on raptinal-induced SYTOX green uptake (**r**). Differences among multiple groups in **d**, **g**, **j**, **l**, **n**, **p**, **r** were analysed by one-way ANOVA, using the Holm–Sidak method for multiple comparisons. Data are mean ± s.d. of three technical (**d**, **g**, **j**, **l**, **n**, **p**) or biological (**r**) replicates. *P* values compare unmutated with mutated constructs. ***$P < 0.0001$. Data are representative of three independent experiments.

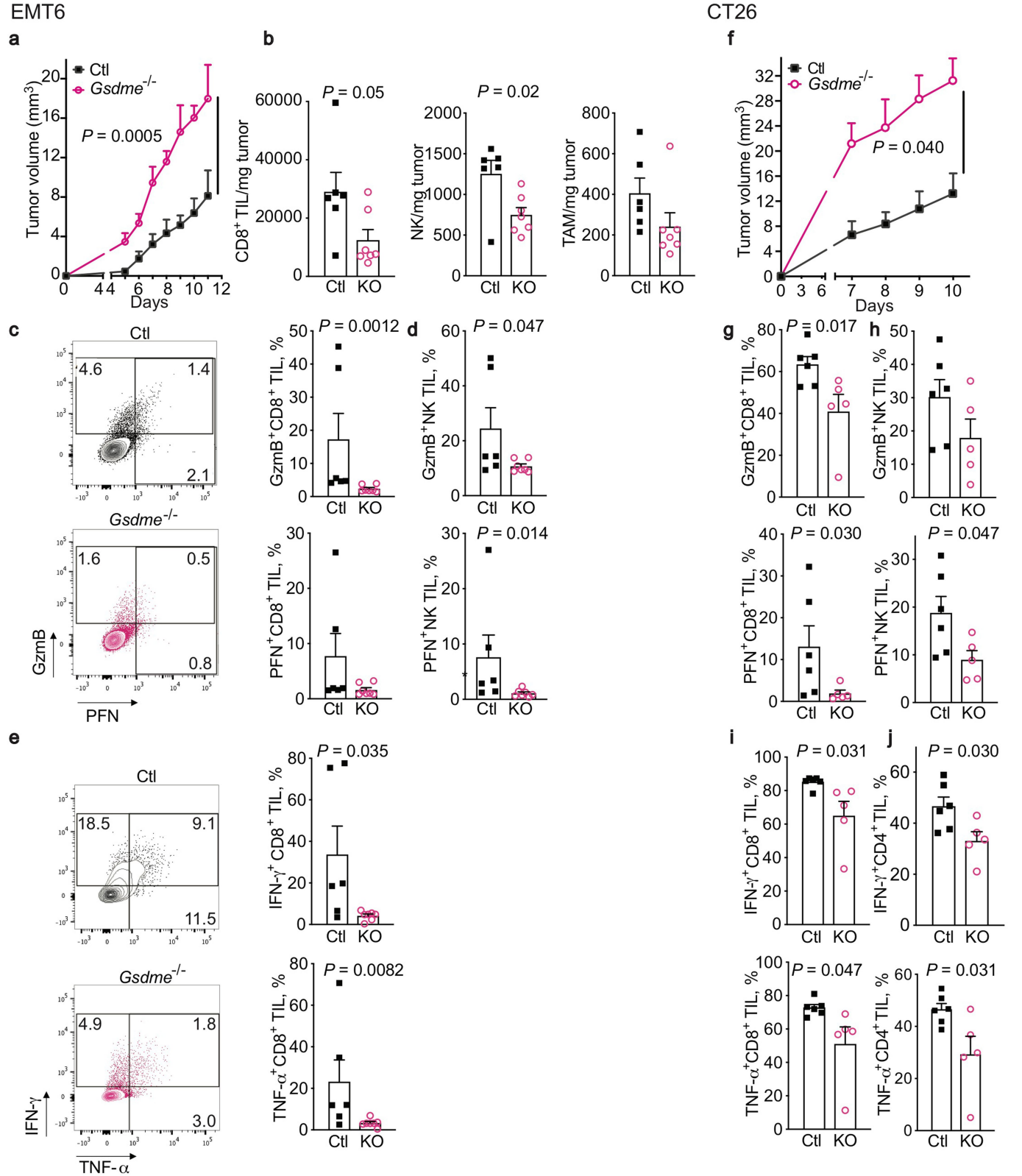

Extended Data Fig. 4 | *Gsdme* knockout in EMT6 and CT26 cells increases tumour growth and reduces immune responses within tumours. **a**–**j**, Comparison of control and *Gsdme*$^{-/-}$ orthotopic EMT6 tumours (control $n = 6$, *Gsdme*$^{-/-}$ $n = 7$) (**a**–**e**) and subcutaneous CT26 tumours (control $n = 6$, *Gsdme*$^{-/-}$ $n = 5$) (**f**–**j**) in BALB/c mice. The effects of knockout are demonstrated in Extended Data Fig. 1. Shown are tumour growth (**a**, **f**); numbers of CD8$^+$ TILs (left), NK cells (middle) and tumour-associated macrophages (right), normalized to tumour weight (**b**); representative flow plots (left) and mean percentage of CD8$^+$ TILs expressing GzmB or PFN (right) (**c**, **g**); mean percentages of NK cells expressing GzmB or PFN (**d**, **h**); and representative flow plots (left) and mean percentage of CD8$^+$ TILs (right, **e**, **i**) and CD4$^+$ TILs (**j**) producing IFNγ or TNF after PMA and ionomycin stimulation. The area under the curve in **a**, **f** and differences between two groups in **b**–**e**, **g**–**j** were compared by two-tailed Student's *t*-test. Data are mean + s.e.m. Data are representative of at least two independent experiments.

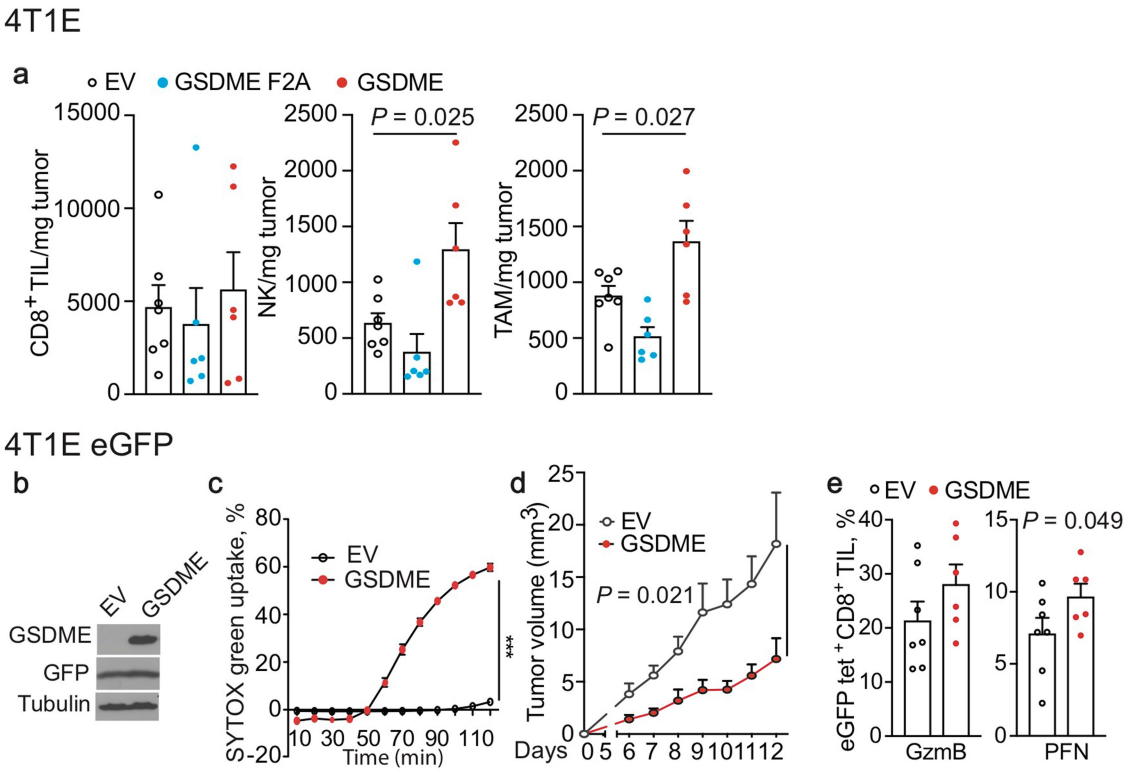

Extended Data Fig. 5 | Effects of GSDME expression on tumour growth and immune responses within 4T1E tumours. a, 4T1E cells stably expressing wild-type mGSDME ($n = 6$ mice per group), the inactive F2A mutant of mGSDME ($n = 6$ mice per group) or an empty vector ($n = 7$ mice per group), implanted in mammary fat pads, were analysed for tumour-infiltrating immune-cell numbers. **b**–**e**, 4T1E cells, stably expressing eGFP and then stably transduced to express mGSDME or empty vector (**b**), were compared for raptinal-induced SYTOX green uptake in vitro (**c**), tumour growth after orthotopic implantation ($n = 7$ mice per group) (**d**), and percentage of $CD8^+$ TILs expressing GzmB or PFN (**e**). Comparisons in **a** were calculated by one-way ANOVA using the Holm–Sidak method for multiple comparisons; comparisons in **e** were calculated by two-tailed Student's *t*-test; comparisons in **c**, **d** were calculated by comparing the difference between the areas under the curve by two-tailed Student's *t*-test. Data shown are mean + s.e.m. ***$P < 0.0001$. All data are representative of two independent experiments.

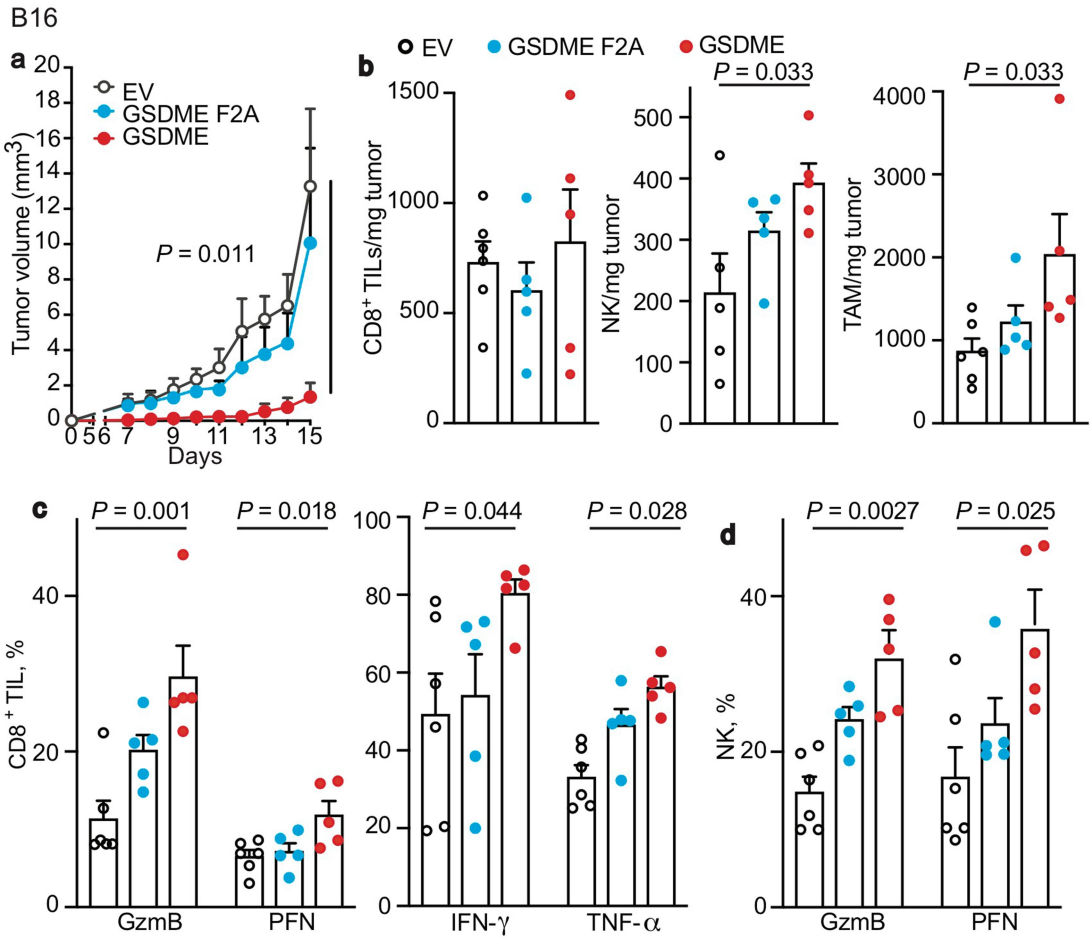

Extended Data Fig. 6 | GSDME overexpression in B16 cells reduces tumour growth and increases immune responses within tumours. a, Tumour growth in C57BL/6 mice that were implanted subcutaneously with B16 cells stably transduced with empty vector ($n = 6$ mice per group) or expressing mGSDME ($n = 8$ mice per group) or inactive F2A GSDME ($n = 5$ mice per group). **b**, Numbers of $CD8^+$ (left) and NK (middle) TILs and tumour-associated macrophages (right) in tumours, normalized to tumour weight. **c**, Percentage of $CD8^+$ TILs expressing GzmB or PFN (left), and IFNγ or TNF after PMA and ionomycin stimulation (right). **d**, Percentage of NK cells expressing GzmB or PFN. The area under the curve of tumour growth curves in **a** was compared by one-way ANOVA with Holm–Sidak correction for type I errors. Comparisons in **b**–**d** were calculated by one-way ANOVA using the Holm–Sidak method for multiple comparisons. Data are mean + s.e.m. All data are representative of at least two independent experiments.

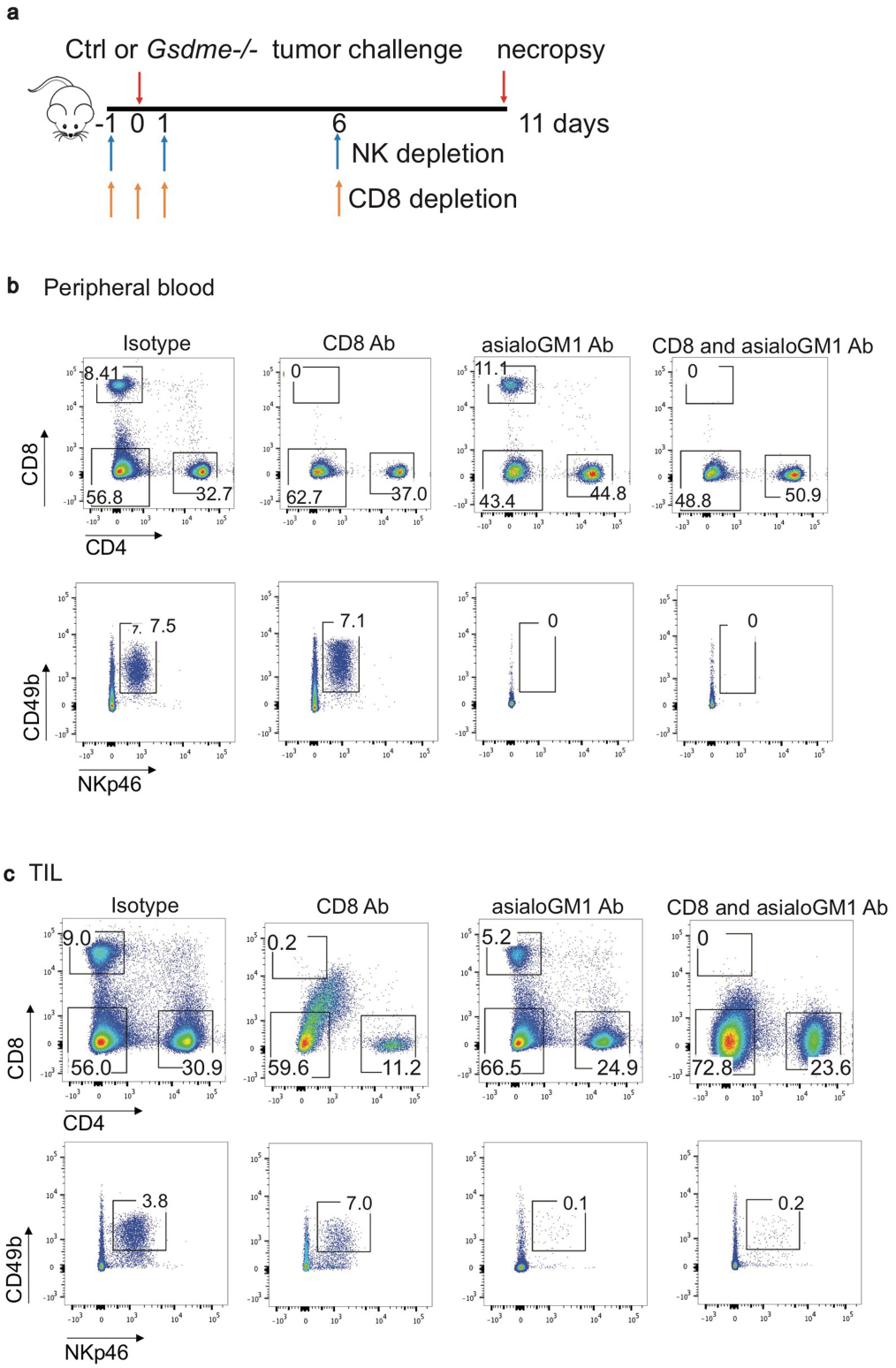

Extended Data Fig. 7 | Depletion of CD8$^+$ T and NK cells in mice bearing EMT6 tumours. a–**c**, Experimental scheme (**a**) and representative flow plots of CD4$^+$ and CD8$^+$ T cells and NK cells in the peripheral blood (**b**) and tumours (**c**) of mice bearing EMT6 tumours treated with isotype control antibody or anti-CD8 and/or anti-asialo-GM1 antibodies in Fig. 2b. Samples were obtained on day 3 (blood) and day 11 (tumours) after tumour challenge. Data are representative of at least two independent experiments.

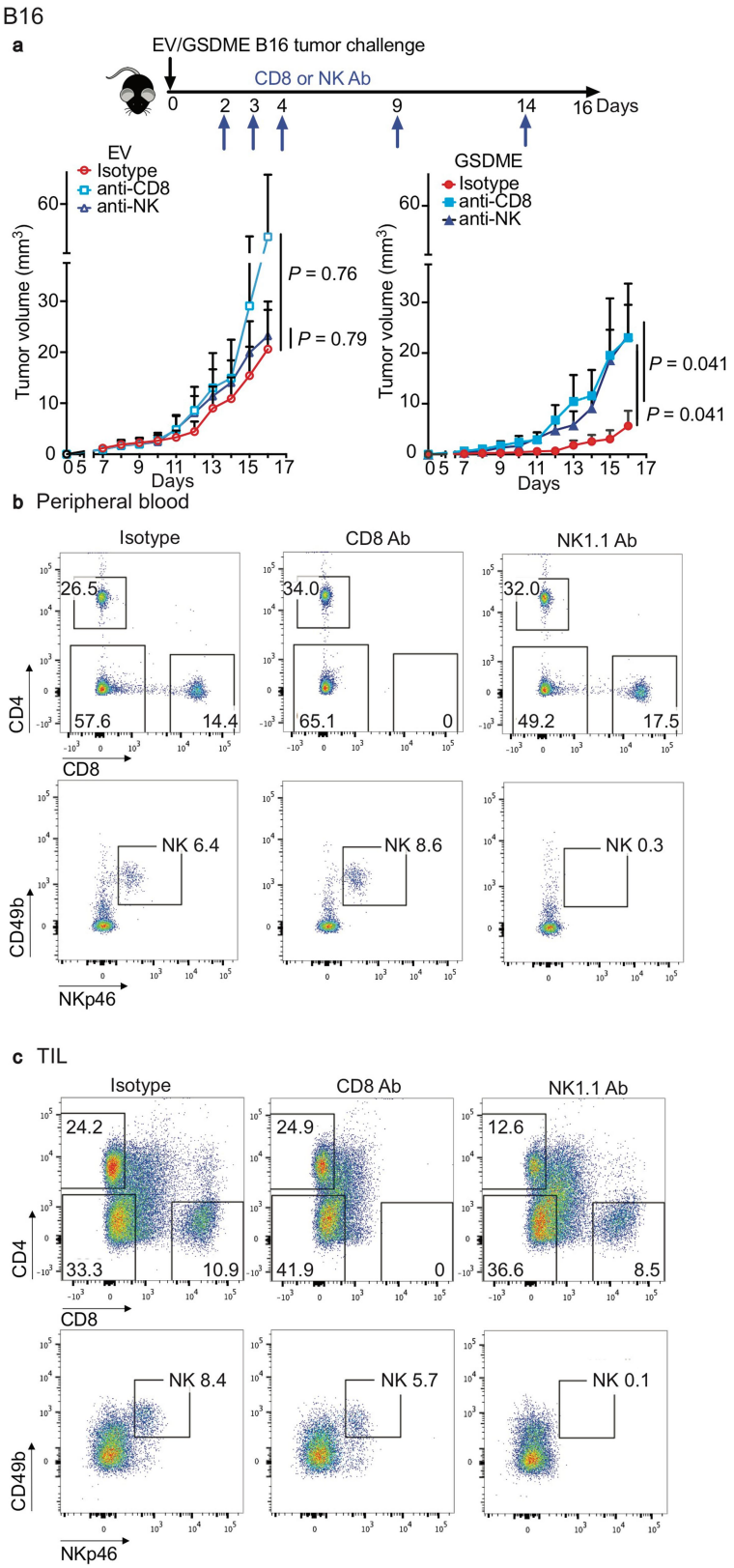

Extended Data Fig. 8 | B16 tumour growth in mice depleted of CD8⁺ or NK cells. a, Experimental scheme and growth of empty vector or mGSDME-positive B16 tumours in mice depleted of CD8⁺ T cells ($n = 6$ mice per group) or NK cells ($n = 6$ mice per group) or treated with an isotype control antibody. Empty vector, $n = 6$ mice per group; mGSDME-positive, $n = 7$ mice per group. **b**, **c**, Antibody depletion was verified by flow cytometry using peripheral blood mononuclear cells (PBMCs) on day 7 after tumour challenge or using TILs at the time of necropsy. Representative flow plots show depletion of CD8⁺ T cells (top) or NK cells (bottom) in the peripheral blood (**b**) and tumours (**c**) of mice bearing B16 empty vector or B16 GSDME tumours treated with isotype control, anti-CD8 or anti-NK1.1 antibodies. The area under the curve of tumour growth curves was compared by one-way ANOVA with Holm–Sidak correction for type I error. Data are mean + s.e.m. All data are representative of two independent experiments.

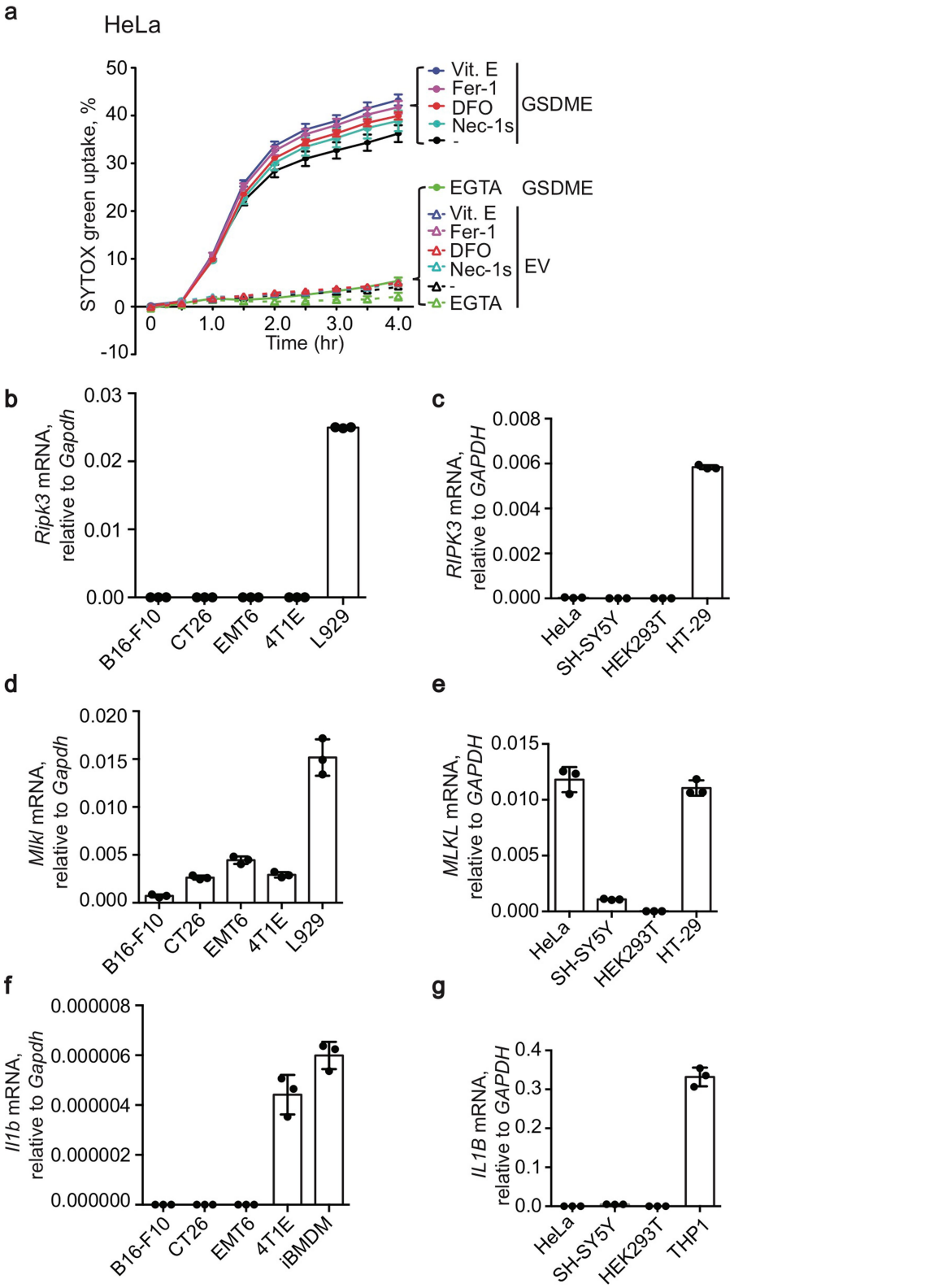

Extended Data Fig. 9 | Necroptosis and ferroptosis are not involved in GSDME-mediated pyroptosis. a, Effect of EGTA, necrostatin-1s (Nec-1s), α-tocopherol (Vit. E), ferrostatin-1 (Fer-1) and desferoxamine (DFO) on YT-cell-induced SYTOX green uptake in EV and hGSDME-positive HeLa cells. **b**–**g**, Cell-death-related gene expression in mouse and human cancer cell lines. *Ripk3* (**b**), *RIPK3* (**c**), *Mlkl* (**d**), *MLKL* (**e**), *Il1b* (**f**) and *IL1B* (**g**) mRNA levels, relative to *Gapdh* or *GAPDH*, respectively, of the indicated mouse (**b**, **d**, **f**) or human (**c**, **e**, **g**) cancer cell lines were assayed by qRT–PCR. Data are mean ± s.d. of biological (**a**) or technical (**b**–**g**) triplicates and are representative of two independent experiments.

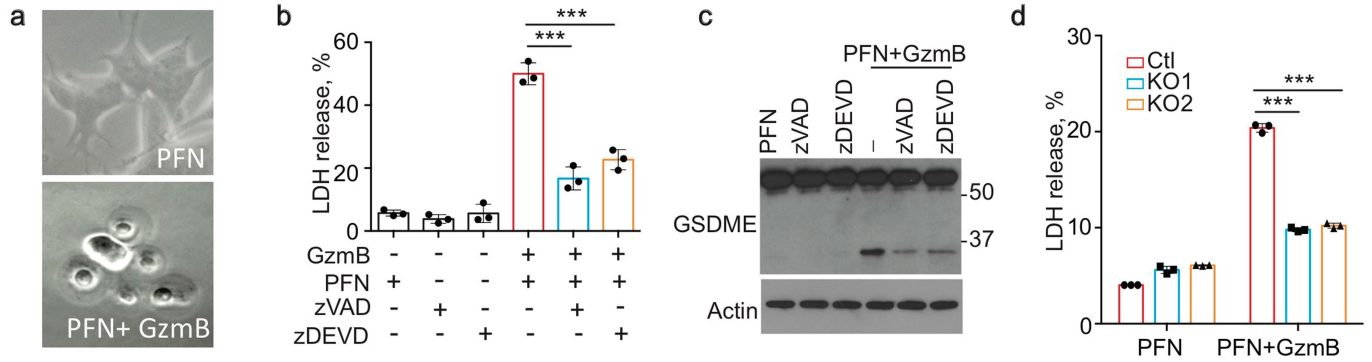

Extended Data Fig. 10 | PFN plus GzmB induce pyroptosis in SH-SY5Y cells. **a**–**c**, SH-SY5Y cells treated with PFN with or without GzmB or medium for 2 h were analysed by microscopy (**a**), immunoblot of cell lysates probed for GSDME and actin (**c**) or LDH release (**b**). In **b**, **c**, treatment was in the presence of 30 μM of caspase inhibitors as indicated. **d**, Effects of *GSDME* knockout on pyroptosis induced by PFN with or without GzmB, assessed after 1 h of treatment by LDH release. Differences among multiple groups in **b**, **d** were analysed by one-way ANOVA using the Holm–Sidak method for multiple comparisons. Data are mean ± s.d. of biological triplicate wells. ***$P < 0.0001$. Data are representative of two independent experiments.

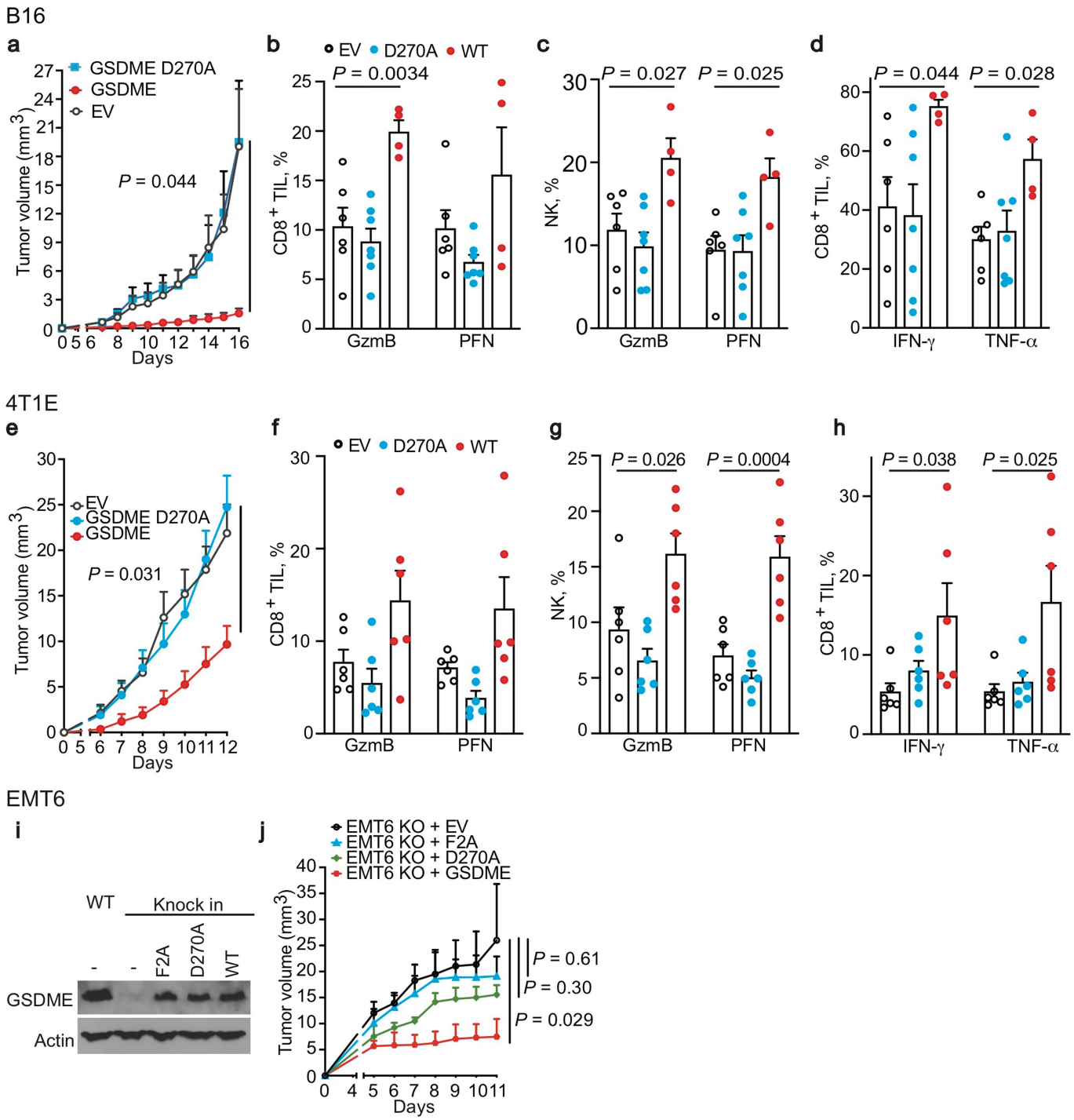

Extended Data Fig. 11 | Uncleavable D270A mutation blocks GSDME-mediated tumour protection and induction of anti-tumour immunity. **a**–**d**, B16 cells stably expressing empty vector ($n = 7$ mice per group), wild-type GSDME ($n = 8$ mice per group) or D270A uncleavable GSDME ($n = 7$ mice per group) were implanted in C57BL/6 mice and followed for tumour growth (**a**) and the functional phenotype of $CD8^+$ and NK TILs (**b**–**d**). Shown are the percentages of $CD8^+$ or NK TILs expressing GzmB or PFN (**b**, **c**) and of $CD8^+$ TILs expressing IFNγ or TNF induced by PMA and ionomycin (**d**). **e**–**h**, 4T1E cells stably expressing empty vector, wild-type or D270A uncleavable GSDME were implanted in syngeneic (BALB/c, $n = 6$ mice per group) mice and followed for tumour growth (**e**) and the functional phenotype of $CD8^+$ and NK TILs (**f**–**h**). Shown are the percentages of $CD8^+$ TILs expressing GzmB or PFN (**f**) or induced by PMA and ionomycin to express IFNγ or TNF (**h**) and of NK TILs expressing GzmB or PFN (**g**). **i**, **j**, *Gsdme*$^{-/-}$ EMT6 cells rescued by transduction with lentiviruses expressing empty vector, wild-type, F2A or D270A GSDME were examined by immunoblot for GSDME expression (**i**) and for tumour growth after orthotopic implantation in BALB/c mice ($n = 8$ mice per group) (**j**). Areas under the curve of tumour growth curves or differences among multiple groups were compared by one-way ANOVA with Holm–Sidak correction for type I error. Data are mean + s.e.m. All data are representative of two independent experiments.

nature research

Corresponding author(s): Judy Lieberman

Last updated by author(s): Dec 30, 2019

Reporting Summary

Nature Research wishes to improve the reproducibility of the work that we publish. This form provides structure for consistency and transparency in reporting. For further information on Nature Research policies, see Authors & Referees and the Editorial Policy Checklist.

Statistics

For all statistical analyses, confirm that the following items are present in the figure legend, table legend, main text, or Methods section.

n/a	Confirmed
☐	☒ The exact sample size (*n*) for each experimental group/condition, given as a discrete number and unit of measurement
☐	☒ A statement on whether measurements were taken from distinct samples or whether the same sample was measured repeatedly
☐	☒ The statistical test(s) used AND whether they are one- or two-sided *Only common tests should be described solely by name; describe more complex techniques in the Methods section.*
☐	☒ A description of all covariates tested
☐	☒ A description of any assumptions or corrections, such as tests of normality and adjustment for multiple comparisons
☐	☒ A full description of the statistical parameters including central tendency (e.g. means) or other basic estimates (e.g. regression coefficient) AND variation (e.g. standard deviation) or associated estimates of uncertainty (e.g. confidence intervals)
☐	☒ For null hypothesis testing, the test statistic (e.g. *F*, *t*, *r*) with confidence intervals, effect sizes, degrees of freedom and *P* value noted *Give P values as exact values whenever suitable.*
☒	☐ For Bayesian analysis, information on the choice of priors and Markov chain Monte Carlo settings
☒	☐ For hierarchical and complex designs, identification of the appropriate level for tests and full reporting of outcomes
☒	☐ Estimates of effect sizes (e.g. Cohen's *d*, Pearson's *r*), indicating how they were calculated

Our web collection on statistics for biologists contains articles on many of the points above.

Software and code

Policy information about availability of computer code

Data collection	SWISS-MODEL was used to model the GSDME-NT structure. Breast cancer and colon cancer RNA-seq expression data were obtained from The Cancer Genome Atlas (TCGA) using the University of California Santa Cruz (UCSC) Xena bioinformatic tool.
Data analysis	Pymol was used to analyze the modeled GSDME-NT structure . Graph design and statistical analysis was performed using Prism V6.0. Protein and DNA sequence analysis were performed by Blast. Images and videos were processed and analyzed by ImageJ Fiji. Flow cytometry data were analyzed by FlowJo v.10.

For manuscripts utilizing custom algorithms or software that are central to the research but not yet described in published literature, software must be made available to editors/reviewers. We strongly encourage code deposition in a community repository (e.g. GitHub). See the Nature Research guidelines for submitting code & software for further information.

Data

Policy information about availability of data

All manuscripts must include a data availability statement. This statement should provide the following information, where applicable:

- Accession codes, unique identifiers, or web links for publicly available datasets
- A list of figures that have associated raw data
- A description of any restrictions on data availability

All data generated or analysed during this study are included in this manuscript and its supplementary information. Source data and uncropped blot images are provided with the paper.

Field-specific reporting

Please select the one below that is the best fit for your research. If you are not sure, read the appropriate sections before making your selection.

☒ Life sciences ☐ Behavioural & social sciences ☐ Ecological, evolutionary & environmental sciences

For a reference copy of the document with all sections, see nature.com/documents/nr-reporting-summary-flat.pdf

Life sciences study design

All studies must disclose on these points even when the disclosure is negative.

Sample size	We chose sample size based on pilot experiments and literature reports in the field to achieve at least 80% power and a two-sided type I error of 5%. The chosen sample size was sufficient to determine statistical significance in our established tumor model.
Data exclusions	No data was excluded from our analysis.
Replication	All experiments were performed at least two or three times with similar results.
Randomization	Mice were randomly allocated to each experimental group.
Blinding	Blinding was not performed due to personnel availability. Random allocation and quantitative measurement using instruments and kits in our experiments minimized biased assessments.

Reporting for specific materials, systems and methods

We require information from authors about some types of materials, experimental systems and methods used in many studies. Here, indicate whether each material, system or method listed is relevant to your study. If you are not sure if a list item applies to your research, read the appropriate section before selecting a response.

Materials & experimental systems

n/a	Involved in the study
☐	☒ Antibodies
☐	☒ Eukaryotic cell lines
☒	☐ Palaeontology
☐	☒ Animals and other organisms
☒	☐ Human research participants
☒	☐ Clinical data

Methods

n/a	Involved in the study
☒	☐ ChIP-seq
☐	☒ Flow cytometry
☒	☐ MRI-based neuroimaging

Antibodies

Antibodies used

anti-GSDME (clone EPR19859, Abcam, Cat#ab215191, Lot#GR3187594-23, 1:1000),
anti-FLAG (clone M2, Sigma, Cat# F1804, Lot# SLCB0524, 1:1000),
anti-caspase-3 (Cell Signaling, Cat#9662S, Lot# 18, 1:1000),
anti-HMGB1 (Abcam, Cat# ab18256, Lot# GR3237475-1, 1:1000),
anti-α-tubulin (clone B-5-1-2, Sigma, Cat#T5168, Lot# 038M4813V, 1:2000),
anti-β-actin (clone JLA20, Developmental Studies Hybridoma Bank, Cat# JLA20,1:2000);
CD45-PerCPCy5.5 (clone 30-F11, BioLgend, Cat#103132, Lot# B276559, 1:100),
CD8-PacBlue (clone 53-6.7, BioLgend, Cat#100728, Lot# B225982, 1:100),
CD8-PerCPCy5.5 (clone 53-6.7, BioLgend, Cat#100734, Lot# B268252, 1:100),
CD8-Alexa700 (clone 53-6.7, BioLgend, Cat#100730, Lot# B246153, 1:100),
CD8-FITC (clone 53-6.7, BioLgend, Cat#100706, Lot# B269214, 1:100),
CD8-APC (clone 53-6.7, BioLgend, Cat# 100712, Lot# B275135, 1:100),
CD4-PE-Cy7 (clone GK 1.5, BioLgend, Cat# 100422, Lot# B258628, 1:100),
CD4-APC (clone GK 1.5, BioLgend, Cat# 100412, Lot# B280301, 1:100),
CD4-PerCPCy5.5 (clone GK 1.5, BioLgend, Cat# 100434, Lot# B248434, 1:100),
CD49b-FITC (clone DX5, BioLgend, Cat# 108906, Lot# B271046, 1:100),
CD49b-PacBlue(clone DX5, BioLgend, Cat# 108918, Lot# B285512, 1:100),
CD49b-PerCPCy5.5 (clone DX5, BioLgend, Cat# 108915, Lot# B245454, 1:100),
NKp46-APC (clone 29A1.4, BioLgend, Cat# 137608, Lot# B252578, 1:100),
CD11b-Alexa700 (clone M1170, BioLgend, Cat# 101222, Lot# B259438, 1:100),
F4/80-PE-Cy7 (clone BM8, BioLgend, Cat# 123114, Lot# B280917, 1:100),
CD44-PerCPCy5.5 (clone IM7, BioLgend, Cat# 103032, Lot# B213817, 1:100),
granzyme B-PacBlue (clone GB11, ThermoFisher Scientific, Cat# 515408, Lot# B271129, 1:10),
Perforin-PE (clone S16009B, BioLegend, Cat# 154406, Lot# B271129, 1:20),

IFN-γ-PacBlue (clone XMG1.2, BioLegend, Cat# 505818, Lot# B234191, 1:100),
TNF-α-PE-Cy7 (clone MP6-XT22, BioLegend, Cat# 506324, Lot# B279986, 1:100),
anti-mouse CD8 (clone 2.43, BioXCell, Cat# BE0061, Lot# 705118J3),
anti-NK1.1 (clone PK136, BioXCell, Cat#BE0036, Lot# 693118J3),
anti-Asialo-GM1 (clone Poly21460, BioLegend, Cat# 146002, Lot# B288357),
InVivoMAb rat IgG2b isotype control, anti-keyhole limpet hemocyanin (clone LTF-2, BioXCell, Cat# BE0090, Lot# 5101/0414).

Validation

All antibodies used in this study are commercially available and are validated by previous publications.
https://www.citeab.com/antibodies/4636686-ab215191-anti-dfna5-gsdme-antibody-epr19859-n-te?des=521b5f54df294288
https://www.citeab.com/antibodies/2304935-f1804-monoclonal-anti-flag-m2?des=f909638f2def0676
https://www.citeab.com/antibodies/126298-9662-caspase-3-antibody?des=309abd94aad8e064
https://www.citeab.com/antibodies/764266-ab18256-anti-hmgb1-antibody-chip-grade?des=df9c5b0866bff6e8
https://www.citeab.com/antibodies/2304940-t5168-monoclonal-anti-tubulin?des=602e33b3b5e2adeb
https://www.citeab.com/antibodies/149691-jla20-acta-antibody-jla20?des=f9809d39f56b7ddf
https://www.citeab.com/antibodies/518038-103132-percp-cyanine5-5-anti-mouse-cd45-30-f11-mon?des=e6fe680346be1442
https://www.citeab.com/antibodies/517236-100728-pacific-blue-anti-mouse-cd8a-53-6-7-monocl?des=8747529d862ff51e
https://www.citeab.com/antibodies/517248-100734-percp-cyanine5-5-anti-mouse-cd8a-53-6-7-mon?des=ff580c0abeba6e09
https://www.citeab.com/antibodies/517240-100730-alexa-fluor-700-anti-mouse-cd8a-53-6-7-mon?des=3bcdc34c54aef032
https://www.citeab.com/antibodies/517201-100706-fitc-anti-mouse-cd8a-53-6-7-monoclonal?des=65e40a1b32c04716
https://www.citeab.com/antibodies/517212-100712-apc-anti-mouse-cd8a-53-6-7-monoclonal?des=e98d89d33090d778
https://www.citeab.com/antibodies/517121-100422-pe-cyanine7-anti-mouse-cd4-gk1-5-monoclonal?des=0279d5010acbc8eb
https://www.citeab.com/antibodies/517114-100412-apc-anti-mouse-cd4-gk1-5-monoclonal?des=ed95416e377df746
https://www.citeab.com/antibodies/517133-100434-percp-cyanine5-5-anti-mouse-cd4-gk1-5-monoc?des=5fe5af49193fe477
https://www.citeab.com/antibodies/517509-108906-fitc-anti-mouse-cd49b-pan-nk-cells-dx5-mo?des=fa9c827b7249a393
https://www.citeab.com/antibodies/517530-108918-pacific-blue-anti-mouse-cd49b-pan-nk-cells?des=a9ac3bb4e6abbd42
https://www.citeab.com/antibodies/517523-108915-percp-cyanine5-5-anti-mouse-cd49b-pan-nk-cell?des=a8bcf3051df74365
https://www.citeab.com/antibodies/519191-137608-apc-anti-mouse-cd335-nkp46-29a1-4-monoclo?des=9c9d80262f7d71b1
https://www.citeab.com/antibodies/517345-101222-alexa-fluor-700-anti-mouse-human-cd11b-m1-70?des=3c9f379c9f209c37
https://www.citeab.com/antibodies/519041-123114-pe-cyanine7-anti-mouse-f4-80-bm8-monoclonal?des=f5313b867fe74faa
https://www.citeab.com/antibodies/517961-103032-percp-cyanine5-5-anti-mouse-human-cd44-im7?des=075fb1aff5449754
https://www.citeab.com/antibodies/1624610-515408-pacific-blue-anti-human-mouse-granzyme-b-gb?des=f8c54797a762128d
https://www.citeab.com/antibodies/4981199-154406-pe-anti-mouse-perforin-s16009b-monoclonal?des=ec14faaf1f13f64f
https://www.citeab.com/antibodies/524989-505818-pacific-blue-anti-mouse-ifn-xmg1-2-monoc?des=7d9c78d0e2ebc53c
https://www.citeab.com/antibodies/525081-506324-pe-cyanine7-anti-mouse-tnf-mp6-xt22-monoc?des=e6f8bacfc916e6dc
https://bxcell.com/product/m-cd8a-2/
https://bxcell.com/product/nk-1-1/
https://www.citeab.com/antibodies/1483798-146002-ultra-leaf-purified-anti-asialo-gm1-antibody?des=d175d0dde948884e
https://bxcell.com/product/rat-igg2b-isotype-control/

Eukaryotic cell lines

Policy information about cell lines

Cell line source(s)

HeLa, HEK293T and EMT6 were purchased from ATCC. 4T1E and 4T1E-eGFP cells were generated in our lab by sorting 4T1 for high E-cadherin expression. 4T1 and 4TO7 cells were kind gifts of Dr. Fred Miller (Wayne State University). B16F10 and CT26 were kindly provided by Dr. Gordon J. Freeman (Dana-Farber Cancer Institute). SH-SY5Y cell was a generous gift of Dr. Yang Shi (Boston Children's Hospital). The YT-Indy NK cell line was a gift of Dr. Zacharie Brahmi (Indiana University).

Authentication

All the cell lines were authenticated by their morphology and functions according to ATCC instructions and published studies.

Mycoplasma contamination

All cells were verified to be free of mycoplasma by PCR.

Commonly misidentified lines
(See ICLAC register)

No commonly misidentified lines were used.

Animals and other organisms

Policy information about studies involving animals; ARRIVE guidelines recommended for reporting animal research

Laboratory animals

Female C57BL/6, BALB/c and NOD.Cg-PrkdcscidIl2rgtm1Wjl/SzJ (NSG) mice (6-8 weeks) were purchased from Jackson Laboratories. Prf1-/- mice (Jackson Laboratories) in the BALB/c background were bred on site.

Wild animals

This study did not involved wild animals.

Field-collected samples

This study did not involved samples collected from the field.

Ethics oversight

All procedures were conducted using protocols approved by the Harvard Medical School IACUC.

Note that full information on the approval of the study protocol must also be provided in the manuscript.

Flow Cytometry

Plots

Confirm that:

☐ The axis labels state the marker and fluorochrome used (e.g. CD4-FITC).

☒ The axis scales are clearly visible. Include numbers along axes only for bottom left plot of group (a 'group' is an analysis of identical markers).

☒ All plots are contour plots with outliers or pseudocolor plots.

☒ A numerical value for number of cells or percentage (with statistics) is provided.

Methodology

Sample preparation	Tumors were harvested from different groups of mice at the time of necropsy. Tumors were cut into small pieces and treated with 2 mg/ml Collagenase D, 100 µg/ml DNase I (both from Sigma) and 2% FBS in RPMI with agitation for 30 min. Tumor fragments were homogenized, filtrated through 70 µm strainers and immune cells were purified by Percoll-gradient centrifugation and washed with Leibovitz's L-15 medium. Peripheral blood samples were collected via facial vein bleeding. Peripheral blood mononuclear cells were purified by Histopaque and washed with Leibovitz's L-15 medium.
Instrument	Flow cytometry was performed by BD FACSCanto II.
Software	Data was acquired by BD FACSDiva software, then analyzed using FlowJo software V.10 (Tri-Star).
Cell population abundance	N/A
Gating strategy	FSC/SSC gates were used to select mononuclear cells. FSC/FSH gates were then used to gate on single cells. Cells were then gated on live cells. Live cells were further gated on CD45+ leukocytes and then different populations of immune cells based on their expression of distinct markers. When needed, isotype control antibody staining was used to define positive/negative cell populations.

☐ Tick this box to confirm that a figure exemplifying the gating strategy is provided in the Supplementary Information.